Investigating the Inhibition of NMDA Receptors by Memantine and Harmonine

Eleanor Johnson

14333688

University of Nottingham

MRes Drug Discovery and Molecular Pharmacology 2022

Supervised by Ian Mellor

Contents

Acknowledgements

Firstly, I would like to extend my deepest gratitude to my supervisor Dr Ian Mellor for his continuous support and guidance throughout the research phase of this project and valuable advice during the thesis writing phase. I also wish to thank the Faculty of Life Sciences at the University of Nottingham for the opportunity to study with them and the facilities made available to me for this research project.

I had the pleasure of working alongside Dennon-Jay Brown Coker and Abdul Rehman and I am very grateful for their support and encouragement throughout the year. Lastly, I would like to thank my family and friends who have provided unwavering support and reassurance through the undulating stages of a research project.

Abstract

Alzheimer's disease (AD), the most common cause of dementia, is a neurodegenerative disease that is mostly characterised by the irreversible and progressive loss of memory. AD exists as two genetically distinct forms, familial and sporadic AD. The pathology of AD is categorised mostly by extracellular amyloid beta plaques and neurofibrillary tangles accompanied by decreased levels of neurotransmitters and neuronal cell death that causes synaptic disruption. Interestingly, increased understanding of the role of amyloid beta plaques in AD has highlighted that they interfere with the glutamatergic pathway, an essential signalling pathway for excitatory neurotransmission in the CNS. Glutamate, after binding to its receptors, is removed from synapses by glutamate transporters, but these transporters are susceptible to binding by amyloid beta plaques. This binding inhibits the reuptake of glutamate, and therefore increases glutamate levels in the synapse. This can cause overactivation of specifically N-methyl-D-Aspartate (NMDA) receptors and increases the level of Ca^{2+} ion influx, causing excitotoxicity of the postsynaptic neurons to produce the neurodegenerative effect.

AD is the largest unmet medical need in neurology. Current drugs improve symptoms, but do not have profound disease-modifying effects. One currently approved drug is memantine, an open channel antagonist that works by inhibiting overactivated NMDA receptors. Memantine works effectively in moderate to severe AD patients to give symptomatic relief. Research into natural NMDA receptor antagonists highlighted the potential of *Harmonia axyridis* alkaloid extract (HAE) as an effective treatment. The main component of HAE is believed to be harmonine (90%). In this study, Two Electrode Voltage Clamp (TEVC) electrophysiology was used to observe the inhibition of GluN1-1a/GluN2A NMDA receptors by memantine, HAE and a harmonine analogue through expression of human RNA injected into *Xenopus laevis* oocyte cells. Concentration- inhibition curves were plotted using the response data recorded to estimate the IC_{50} at several holding potentials (V_h) including -25 mV, -50 mV, -75 mV and -100 mV.

Memantine, HAE and the harmonine analogue were all found to inhibit the NMDA receptors in a concentration- and voltage-dependent manner. Memantine and the

harmonine analogue demonstrated complete inhibition of the NMDA receptor response when applied at the highest concentration (10^{-4} M). HAE showed a large degree of response inhibition when applied at the highest concentration (3 μg/mL). IC_{50} values for the inhibition of the NMDA receptor response at V_h -75mV were 0.68 μM for memantine, 2.44 μM for HAE and 1.08 μM for the harmonine analogue. Overall, all compounds showed a similar level of NMDA receptor response inhibition and therefore harmonine and harmonine analogues could be further explored for their potential use as therapeutic drug treatments for AD.

1 Introduction

1.1 Neurodegenerative diseases and Alzheimer's Disease pathology

Alzheimer's disease (AD) is the most common form of age-related neurodegenerative disease and is caused by the chronic progression of neurodegenerative damage. AD is estimated to cause around 60-70% of dementia cases and is most common in individuals over the age of 60 (Holtzman et al., 2011). The disease causes synaptic and metabolic dysfunction before leading to complete cell death (Selkoe, 2002). The most characteristic and recognisable early symptom of AD is short-term memory loss (amnesia) (Olivares et al., 2012). The amnesia is then followed by complete dementia which includes cognitive decline, further memory decline and also impaired performance of daily activities, speech and visual-spatial perception (Draper, 2013; Holtzman et al., 2011).

The progression of AD is believed to be due to gradual damage to the structure and function of the hippocampus and neocortex, the main brain areas involved in memory and cognition (Mota et al., 2014). Extensive research into the gradual damage processes of AD identified common pathological changes, with a leading hypothesis centring on neurotoxic protein deposits in the brain (Parsons et al., 2013). These deposits include the accumulation of extracellular amyloid beta plaques (Aβ) composed of amyloid beta peptides, and the accumulation of neurofibrillary tangles (NFTs) that are comprised of misfolded and hyperphosphorylated tau proteins (Olivares et al., 2012; Navarro et al., 2018; Mota et al., 2014). These protein deposits are also accompanied by impairment of neurotransmitter systems through decreased levels of neurotransmitters and the loss of neurones and synapses. In the earliest stages of AD onset, the Aβ plaques and NFTs are prevalent in the entorhinal cortex (Khan et al., 2014). These authors found that the NFTs initially accumulate and then make the entorhinal cortex vulnerable to Aβ plaque accumulation, and thus enabling further neurone damage. AD then develops as the proteins begin to spread to different areas of the brain, including the hippocampus, adjacent limbic and temporal cortex, the association isocortex, and finally to primary sensory cortex (Vogel et al., 2020). AD in a patient can be confirmed by the presence of Aβ plaques and NFTs during the autopsy, however in recent years both pathological proteins can be

observed in the brains of living humans using positron emission tomography (PET) which enables the recognition of the diseases before death and even before symptoms may begin (Villemagne et al., 2018).

AD exists as two genetically distinct forms, familial AD (also known as early onset AD) and sporadic AD (also known as late onset AD) (Julia and Goate, 2017). Familial AD is characterised by the onset of the disease before the age of 60 and is inherited in a Mendelian fashion, with little influence from the environment. In contrast to this, sporadic AD, which is mostly seen in individuals over the age of 60 and is thought to cause around 90% of AD cases, is largely influenced by environmental factors, and genetics has less of an effect on development. The genetic aspect of sporadic AD is mainly associated with epsilon allele in the apolipoprotein E gene (APOE4). However, other genetic factors are continually researched as many carriers of the APOE epsilon allele live into their 90s, suggesting the existence of other genetic and/or environmental risk factors (Selkoe and Hardy, 2016; Bekris et al., 2011). Sporadic AD is also largely influenced by faulty Aβ degradation systems (Selkoe and Hardy, 2016). The small fraction of patients that develop familial AD are believed to suffer from a number of inherited mutations in one of three genes; the β-amyloid precursor protein (APP) gene in chromosome 21, presenilin-1 (PS1) in chromosome 14 and presenilin-2 (PS2) in chromosome 1 (21, 177 and 14 mutations respectively) (Olivares et al., 2012). A commonality of these mutations is that they all, through different routes, increase the generation of Aβ, specifically the ratio of Aβ42 (42 amino acid residues): Aβ40 (40 residues) (Yin et al., 2007). This is comparable to sporadic AD, where the onset cause is thought to instigate a gradual rise in extracellular Aβ42 plaques, contributed to by defects in the Aβ clearance mechanisms (Selkoe and Hardy, 2016). These high levels of extracellular Aβ42 plaques transpire to cause neuronal and synaptic dysfunction and neuronal loss. From many of the findings to date it can be concluded that the Aβ plaque hypothesis has become the more dominant model of AD pathogenesis.

1.2 Aβ Plaques and the glutamatergic system in Alzheimer's Disease

Aβ plaques are known to be formed by the amyloidogenic processing and sequential cleaving of the metalloprotein APP by two membrane bound endoproteases (Murpy

and LeVine III, 2010). APP is a ubiquitously expressed transmembrane protein that is processed by either 'amyloidogenic' (AD) and 'non-amyloidogenic' (healthy individuals) processing (Pająk et al., 2016). During amyloidogenic processing, the full-length APP is endocytosed before being cleaved by β-secretase (BACE1) to release soluble APPβ (sAPPβ) and the amino terminus of Aβ in the APP C-terminal fragment 99 (APP-CTF999) (Figure 1). Aβ is then cleaved by γ-secretase to produce Aβ40, Aβ42, and APP intracellular domain (AICD). In healthy individuals, non-amyloidogenic processing occurs and during this, α-secretase cleaves APP to produce the soluble fragment sAPP-α, and the APP C-terminal fragment 83 (APP-CTF83). APP-CTF83 is then cleaved by γ-secretase to release the APP intracellular domain (AICD) and P3 fragment. The APP, PS1 and PS2 mutations in familial AD are thought to increase the levels of the amyloidogenic processing and sporadic AD causes a gradual rise of the Aβ42 levels in the brain through failure of Aβ clearance mechanisms (Selkoe and Hardy, 2016). These Aβ40 and Aβ42 plaques are thought to have the ability to negatively modulate the glutamatergic system which is key within learning and memory (Findley et al., 2019). The glutamatergic system involves the synthesis of glutamate from glutamine by glutaminase in the presynaptic neuron (Niciu et al., 2012). Glutamate is the principle excitatory neurotransmitter in the central nervous system, it is found in around 80% of neurons, particularly within the cortex and hippocampal regions of the brain (Danysz et al., 2000). Once the glutamate is formed in the presynaptic neurone it is transported to the synaptic terminals where vesicular glutamate transporter-1/2 packages it into vesicles to release upon presynaptic depolarisation (Figure 2). Subsequently after release, glutamate binds for short periods to the post-synaptic ionotropic glutamate receptors (iGluRs) and then it is cleared from the synapse by high efficiency excitatory amino acid transporters (EAATs) that are located primarily on astrocytes (Chen and Lipton, 2006; Niciu et al., 2012). Upon uptake into the astrocytes, the glutamate is converted into glutamine by glutamine synthetase and then transported back to the presynaptic neuron to contribute again to the cycle.

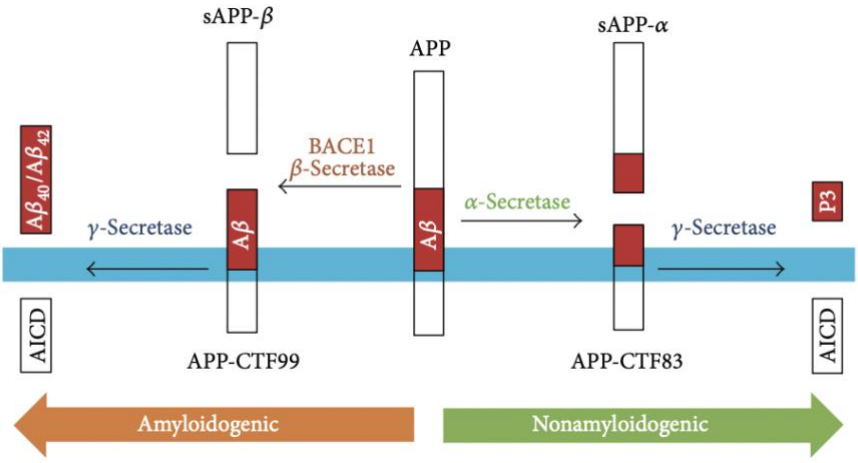

Figure 1. Diagram to show the amyloidogenic (AD) and nonamyloidogenic (healthy individuals) processing pathways. In the amyloidogenic processing, the transmembrane protein APP (membrane indicated in blue) is cleaved in the middle of the Aβ region (red) by β-secretase (BACE1) to release soluble APP-fragment sAPP-β and the APP C-terminal fragment 99 (APP-CTF99). APP-CTF99 is then cleaved by γ-secretase to release the APP intracellular domain (AICD), Aβ40 and Aβ42. In the nonamyloidogenic pathway, α-secretase cleaves in the middle of the β-amyloid (Aβ) region to release the soluble APP-fragment sAPP-α and the APP C-terminal fragment 83 (APP-CTF83). APP-CTF83 is then cleaved by γ-secretase to release the APP intracellular domain (AICD) and P3 fragment. (Figure taken from (Pająk et al., 2016)).

Excitatory synaptic neurotransmission relies on the release of glutamate from the presynaptic terminals to bind and activate the postsynaptic iGluRs (Blanke and VanDongen, 2008). To avoid excess glutamate accumulation there needs to be regulation of the glutamatergic system, as excessive release or insufficient glutamate removal will result in the overactivation of the postsynaptic iGluRs, namely, N-Methyl-D-Aspartate (NMDA) receptors (NMDAR) (Ezza and Khadrawyb, 2014). Aβ plaques have been reported to bind to glutamate transporters in the synaptic cleft to inhibit the uptake of glutamate, increasing the concentration of glutamate in the synapse (Mucke and Selkoe, 2012). The increased levels of glutamate in the synapse can increasingly activate the NMDARs which can lead to the synaptic dysfunction and the loss of synapses and neurones that is often recognised in early AD stages (Chen and Lipton, 2006). Additionally, Alberdi et al. (2010) reported that Aβ plaques directly activated NMDARs in neurons *in vitro* and in entorhinal cortex–hippocampus organotypic cultures. Through this binding there was an increase in the Ca^{2+} ion influx into the neurons which causes apoptotic cell death. Thus this information highlights the connection between Aβ accumulation, glutamate toxicity

and AD pathology but the exact role of Aβ and NMDARs in AD remains not fully understood (Olivares et al., 2012)

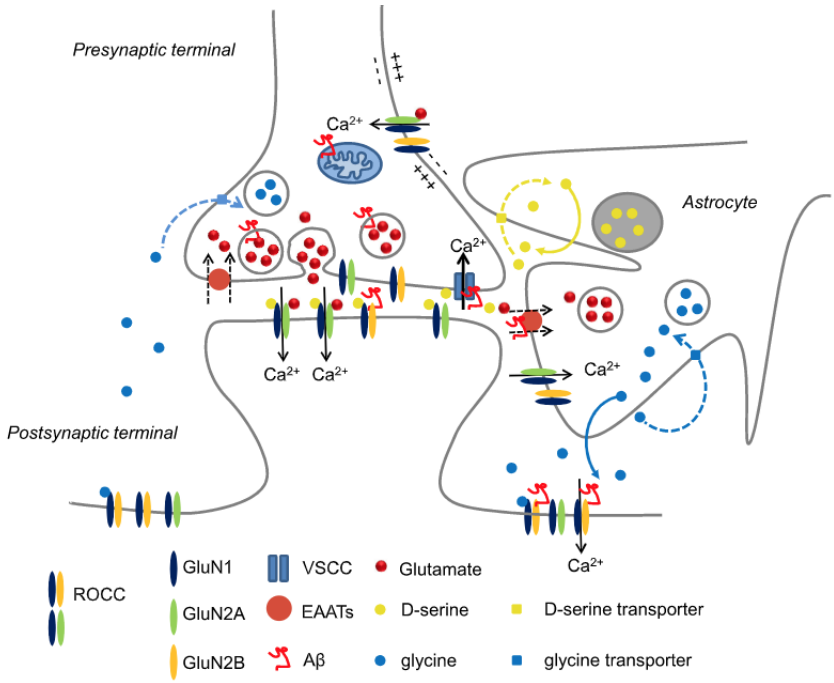

Figure 2. A tripartite glutamatergic synapse. Upon presynaptic depolarisation, glutamate is released into the synapse and activates NMDARs localised on the postsynaptic membrane. Activation causes Ca^{2+} ions to influx into the postsynaptic neuron to propagate an action potential. After activation, glutamate can be removed from the synapse and the postsynaptic neuron by surrounding astrocytes through EAATs and here the glutamate is stored in vesicles, preventing excitotoxicity. In conditions of excessive glutamate release or inhibited glutamate uptake, often due to the presence of Aβ plaques, the NMDARs can become excessively activated (Figure taken from (Zhang et al., 2016))

1.3 Additional Alzheimer's Disease hypotheses; Cholinergic system

Another proposed explanation for the occurrence of AD is described through the cholinergic hypothesis. This links AD to detrimental changes in the cholinergic system, which when impaired, effects all aspects of cognition, behaviour, and cortical and hippocampal information processing. This is because the cholinergic system has major roles, through cholinergic neurotransmission, within modulating these important neural functions (Bartus, 2000; Ferreira-Vieira et al., 2016). The system impairments occur due to decreased levels of the enzyme choline acetyltransferase (ChAT) in the brain of AD sufferers (Fotiou et al., 2015). This was first proposed in 1976 by Davies and Maloney who compared 20 AD affected and unaffected brains to see the activity of multiple key enzymes that are involved in the synthesis of different neurotransmitters (Davies and Maloney, 1976). From this they found ChAT

activity was greatly reduced in AD brains in the amygdala, hippocampus, and cortex, whilst the other key enzymes were found to be working at normal regulated levels. ChAT is responsible for the synthesis of the neurotransmitter acetylcholine (ACh), vital within the central and peripheral nervous system. Therefore, the impaired activity of ChAT was decreasing the amount of ACh available for synaptic transmission. The involvement of the cholinergic system in AD was supported by Terry and Buccafusco (2003) who used cholinergic antagonists to show that they impaired memory levels in animals. They also studied damages/lesions that interfered with cholinergic input from the basal forebrain to the neocortex and hippocampus, here they observed memory deficits in both humans and animals. Additionally, analyses by Sims et al. (1983) used biopsy samples from the neocortex and found that ChAT activity, and therefore ACh synthesis, was reduced in patients with AD. There is also thought that Aβ may somehow interact with ACh to depress the release, synthesis, and the axonal transport of it but this is not yet very well understood (Auld et al., 2002; Nyakas et al., 2011). Increasing the understanding of the role of the cholinergic and glutamatergic systems within AD will open many avenues for progressing AD therapeutic treatments.

1.4 NMDARs and the impact of overactivation

As aforementioned, NMDARs are a subclass of iGluRs; a group of ligand gated ion channels activated mainly by glutamate at their agonist recognition site (Traynelis et al., 2010). NMDARs have a transmembrane ion permeation pathway (channel) and a gating mechanism that undergoes conformational changes to open or close the pore depending on the presence of neurotransmitters glutamate and glycine. This is one unique factor of NMDARs; their activation requires the binding of glutamate, main excitatory agonist, and glycine, a co-agonist (Blanke and VanDongen, 2008). NMDARs are critical receptors that play a role in neuronal development, synaptic plasticity, learning, and memory in the mammalian CNS (Traynelis et al., 2010). These receptors are capable of these roles as they possess a high affinity for the excitatory glutamate, slow kinetics of activation and deactivation, pronounced voltage dependency due to an external Mg^{2+} ion block and high permeability to Ca^{2+} ions (Blanke and VanDongen, 2008).

Under normal conditions of synaptic transmission, where there is regulated levels of glutamate released from microglia and presynaptic neurons, the NMDAR channel is blocked by Mg^{2+} ions that sit within the pore during resting potential (Olivares et al., 2012). At this time, more than 90% of the NMDAR channels are reported to be blocked by Mg^{2+} ions (Johnson and Kotermanski, 2006). During regular postsynaptic activation, causing sufficient membrane depolarisation from resting membrane potential at -70mV to -50mV, the Mg^{2+} ion is removed for a small duration, whilst the glutamate and glycine is bound, to allow for the influx of Ca^{2+} ions through the receptor before the Mg^{2+} block is then positioned back. Sequentially, Ca^{2+} ions activate signaling cascades within the postsynaptic neurons that produce synaptic plasticity, such as long term potentiation (Liu et al., 2019). As aforementioned, sometimes the NMDARs can be overactivated by low levels of glutamate that remain in the synapse due to inhibited levels of glutamate uptake. Under these pathological conditions, there is a detrimental rise in Ca^{2+} ion influx that can cause excitotoxicity of the postsynaptic neurones, producing a neurodegenerative effect (Fendt and Verstreken, 2017).

Interestingly, NMDARs aren't activated by low frequency single synaptic events (Blanke and VanDongen, 2008). As discussed, when an action potential arrives at the presynaptic terminal, glutamate is released into the synapse (Rothstein et al., 1994; Huang and Bergles, 2004). The efficient removal of the glutamate into nearby astrocytes occurs after about a millisecond and therefore, during all synaptic transmission, including low frequency transmission, the glutamate is only briefly available for NMDAR binding (Blanke and VanDongen, 2008). To compensate for the brief agonist availability, NMDARs have a relatively high affinity for glutamate and therefore the millisecond long neurotransmitter pulses should hypothetically be efficient to activate NMDARs through the neurotransmitter binding. However, despite the high affinity, single synaptic events do not activate the NMDARs due to another NMDAR property; they are voltage dependent receptors. As aforementioned, at resting potentials the NMDARs are blocked by Mg^{2+} ions that are tightly bound to the receptor pore to prevent ion permeation into the postsynaptic neuron (Nowak et al., 1984; Mayer et al., 1984). The tight binding occurs because the Mg^{2+} ions are present in millimolar concentrations in the external milieu of neurons and are only present in micromolar concentrations intracellularly, resulting in the net inward

driving force of Mg^{2+} ions at negative resting potentials of the internal membrane (Blanke and VanDongen, 2008). Therefore, to remove these Mg^{2+} ions there needs to be postsynaptic depolarisation of sufficient amplitude and duration (reaching around -50mV). The sufficient depolarisation is likely due to the activation of co-localised AMPA and kainate receptors, other subclasses of iGluRs, by glutamate which contributes to a change in the voltage field across the NMDAR channel, and this sequentially forces the Mg^{2+} ions out to allow for the flow of permeant ions (Johnson and Kotermanski, 2006). This necessity for NMDARs to have sufficient membrane depolarisation, to remove the Mg^{2+} block, and the necessity of presynaptic glutamate release has led to the receptors often being referred to as molecular coincidence detectors (Johnson and Kotermanski, 2006). However, there is thought that when the receptors are exposed to low levels of glutamate that remain in the synapse during pathological conditions, this is sufficient to remove the Mg^{2+} ion block and therefore this leads to excessive activation and a continuous flow of Ca^{2+} ions into the postsynaptic neurone that creates a 'background noise' of NMDAR activation during pathological rest (Parsons et al., 2013)

NMDARs are also unusual in that they have very high Ca^{2+} ion permeability; the ion channel is 10 times more permeable to Ca^{2+} ions than it is to Na^{2+} ions (Hartmann and Konnerth, 2005). As aforementioned, the activation of the NMDARs by neurotransmitter binding initiates the influx of Ca^{2+} ions through the receptor and this influx is vital in the propagation of postsynaptic signaling pathways (Hartmann and Konnerth, 2005). These pathways include the stabilisation of synaptic connection and long-term depression/potentiation of synaptic strength (Olney, 2003; Hardingham and Bading, 2003; Nicoll and Malenka, 1999). Therefore, we can see that long lasting effects on synaptic strengthening and weakening, which plays a huge role in memory and cognition, are dependent on, and mediated by, Ca^{2+} ion influx through NMDARs (Blanke and VanDongen, 2008).

It is believed that glutamate and glycine have similar roles in NMDAR activation (Blanke and VanDongen, 2008). However, when glutamate is released from specific presynaptic terminals, low concentrations of ambient glycine that are present in the synapse are thought to be sufficient for receptor activation. Therefore, it can be said that glycine plays a more modulatory role *in vivo*. The importance of ambient glycine

in NMDAR activation was highlighted in experiments conducted with transgenic mice (Blanke and VanDongen, 2008; Ballard et al., 2002). These mice carried mutant alleles that resulted in lowered glycine affinity. As a result, the mice displayed a spectrum of cognitive and learning defects and confirmed the role of glycine in NMDAR activation. This experiment also highlighted the role of NMDARs in cognition and learning. It is also thought that glycine may have the ability to partially activate NMDARs in the absence of glutamate, but this is poorly studied. Activation primarily by glycine was tested by expressing NMDARs in *Xenopus laevis* oocytes and here, 10 μM glycine was seen to activate the receptor by a few percent (Jones et al., 2002). Studies have also shown that alongside glycine, D-serine can work as a partial agonist, but it is not yet confirmed as to whether it can partially activate in the absence of glutamate and overall is not very well studied (Blanke and VanDongen, 2008; Wolosker, 2006).

1.5 NMDAR structure

NMDARs are heterotetrametric protein complexes composed of two pairs of subunits from seven homologous genes (Figure 3a) (Blanke and VanDongen, 2008). These seven genes create three subunit families, GluN1, GluN2 (A-D) and GluN3 (A-B). In mammals these subunits are encoded for by these seven genes: GRIN1, GRIN2A, GRIN2B, GRIN2C, GRIN2D, GRIN3A AND GRIN3B (Kehoe et al., 2013; Yin et al., 2007). Interestingly, the GluN1 subunit gene consists of 22 exons and exon 5, 21 and 22 can be alternatively spliced to create eight isoforms (Monaghan and Jane, 2009). These splice variants are GluN1-1a, 1-1b, 1-2a, 1-2b, 1-3a, 1-3b, 1-4a, 1-4b. GluN1-1a is the most abundantly expressed form (Stephenson, 2006). The four subunits that form a functional NMDAR are assembled around the transmembrane ion permeation pathway (the pore) (Blanke and VanDongen, 2008). NMDARs must contain an obligatory GluN1 subunit and at least one modulatory GluN2 subunit to be classified as a functional NMDAR (Sasaki et al., 2002; Monyer et al., 1994). This is due to knowledge, from mutagenesis studies, that the GluN1 subunits contain the binding sites for glycine molecules and the GluN2 subunits contain the binding site for glutamate (Vieira et al., 2020). The GluN1-1a/GluN2A and GluN1-1a/GluN2B subunit receptor combination is the most common combination of NMDARs found in mature neurons in the vertebrate brain (Waxman and Lynch, 2005). Recent studies

have shown that the GluN3 subunits can also loosely bind glycine molecules (Grand et al., 2018). This subunit can substitute for one of the GluN2 subunits to still form a tri-heteromeric NMDAR, with thinking that if the GluN3 subunit is present then it will likely modulate the receptor properties. Research has shown that the GluN3 subunits reduce the susceptibility of NMDARs to Mg^{2+} blockade and reduce Ca^{2+} permeability (Kvist et al., 2013). GluN3 subunits could also technically replace both GluN2 subunits to form a glycine-activated receptor, but this would then result in a different receptor all together than an NMDAR (Blanke and VanDongen, 2008).

All NMDAR subunits share a common membrane topology that is conserved throughout the iGluR family. They have a large extracellular amino terminal domain (ATD), an intracellular C terminal domain (CTD), an agonist binding domain (ABD), three transmembrane segments (M1, M3 and M4) and a membrane re-entrant pore loop (M2) (Figure 3a, 3b). The M2 loop is part of the channel pore and contributes to the selectivity filter of the channel (Figure 3c). It also facilitates the Mg^{2+} ion blockade and therefore controls the Ca^{2+} ion permeability of the channel (Kumar, 2015). Near the tip of this loop is a critical asparagine residue (Q/R/N site) that is important for the binding of several channel blockers (Monaghan and Jane, 2009; Huettner, 2015). Single amino acid substitutions confirmed that interactions at or near the Q/R/N site are involved in the Ca^{2+} ion permeability and Mg^{2+} block (Huettner, 2015). Ca^{2+} permeability is also thought to be defined by the DRPEER motif, which is located C terminal to M3 and is unique to GluN1 subunits. Based on measurements of fractional Ca^{2+} currents, under physiological conditions, Watanabe et al. (2002) showed that DRPEER was a key determinant of the high Ca^{2+} influx mediated by NMDAR channels. It is thought that the three negative charges (one aspartate and two glutamate residues) and the one positive charge (the first arginine residue) of the DRPEER motif are exposed to the water interface and therefore influence ion conduction across the NMDARs (Wollmuth and Sobolevsky, 2004).

The main gating domain in glutamate receptors seems to be the M3 segment, it forms a bundle helical crossing, or a gate, at the extracellular end of the transmembrane segment (Figure 3c) (Jones et al., 2002; Wollmuth, 2019). Around the helical bundle there is the SYTANLAAF motif, which is the most highly conserved motif in iGluRs and forms elements of the activation gate (Figure 3c) (Sobolevsky et

al., 2009). This motif is also the site of the *lurcher* mutation (SYTANL**A**AF) that initially identified the M3 segment as a gating element (Zuo et al., 1997). The basic opening mechanism of the M3 gate is believed to include mechanical pulling; when the agonist binds to the LBD it is thought to pull the M3 segment away from the central axis of the pore and cause the channel to open (Wollmuth, 2019). Interactions between the GluN1 and co-assembling GluN2/3 subunits through the ABD has been proven crucial for defining receptor deactivation mechanisms that are unique for each combination of NMDAR (Bledsoe et al., 2017).

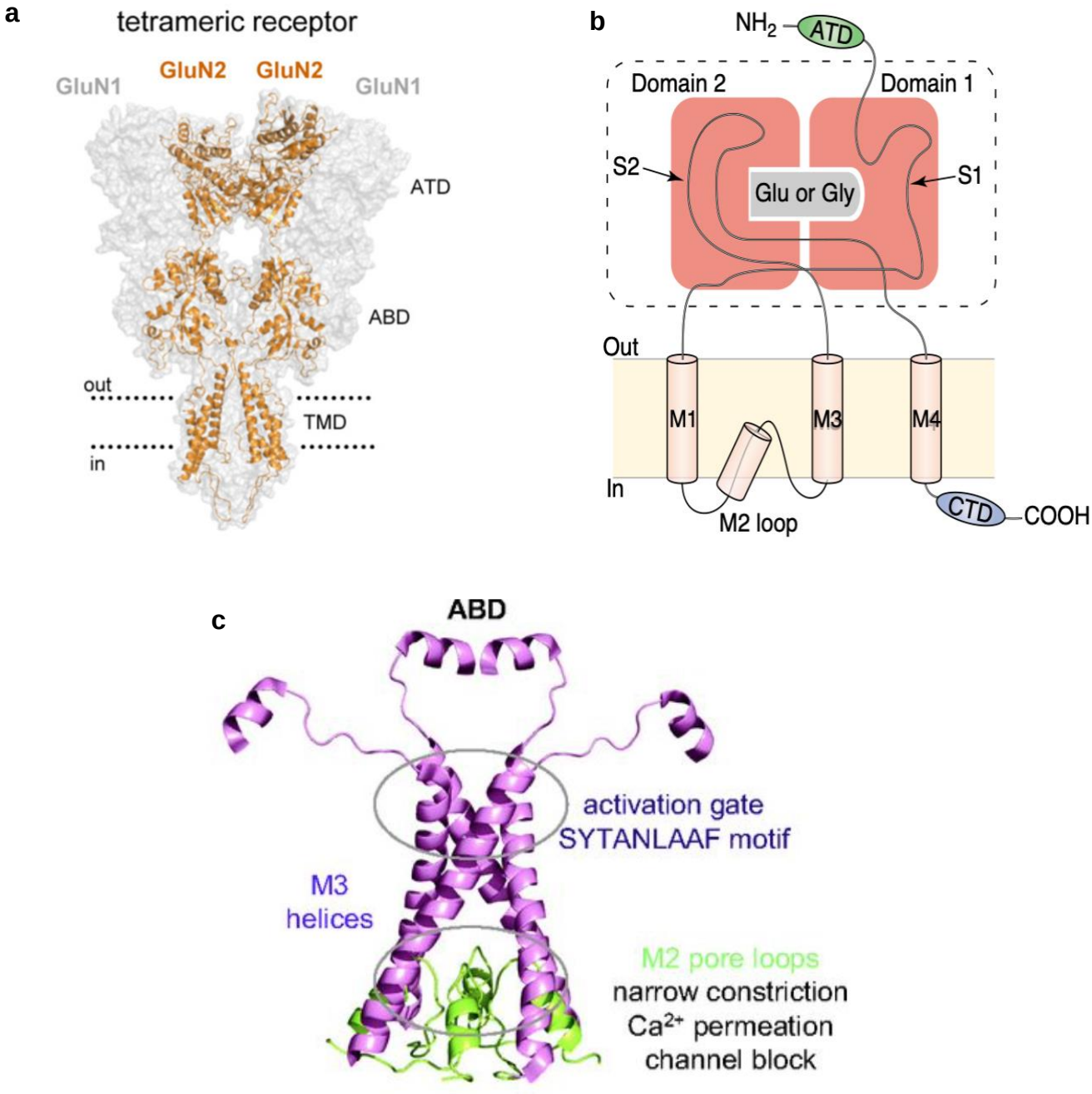

Figure 3. a) Model of the NMDAR based on the crystal structure of the membrane spanning Glu2A AMPA receptor ((Sobolevsky et al., 2009)), showing the tetrameric arrangement of two GluN1 and two GluN2 subunits. The intracellular carboxyl-terminal domain (CTD) was not part of the crystal structure and is not included from the figure. b) Figure showing single subunit NMDAR with the four domains, the extracellular amino-terminal domain (ATD), the agonist binding domain (ABD) (domain 1 and 2 in red), the transmembrane domain (composed of the transmembrane segments M1, M3, and M4, as well as the membrane re-entrant loop M2), and the intracellular carboxyl-terminal domain (CTD). (Figure taken from ((Wollmuth and Sobolevsky, 2004). c) Model of the key functional features of the TMD pore showing the SYTANLAAF motif around the M3 segment and showing the M3 segment forming an activation gate at the extracellular end of the transmembrane segment. The M2 pore loop forms the narrow constriction, controlling the Ca^{2+} ion permeation. (Figure taken from ((Hansen et al., 2021)).

The structure of neurotransmitter binding sites (ABDs) are very similar for both glycine and glutamate (Blanke and VanDongen, 2008). The glycine binding site in GluN1 is formed by the region that precedes segment M1 (in the S1 domain) and the extracellular loop region between segments M3 and M4 (S2 domain) (Figure 3b) (Yamakura and Shimoji, 1999). The glutamate binding site resides in homologous regions on GluN2 subunits. S1 is a sequence of 120 amino acids located between the ATD and the first transmembrane domain (M1). Together, S1 and S2 form a bilobed structure with structural homology to the bacterial leucine–arginine–ornithine binding protein (LAOBP) (Stern-Bach et al., 1994). Agonist affinities and antagonist sensitivities of heteromeric NMDAR channels are determined by the nature of the GluN2 subunits, the four glutamate-binding GluN2A-D subunits provide the CNS with a means of controlling NMDAR properties (Hansen et al., 2018). Research conducted by Yamakura and Shimoji (1999) found the EC_{50} values for glutamate to be 1.7, 0.8, 0.7 and 0.4 μM for the GluN1-1a/GluN2A, GluN1-1a/GluN2B, GluN1-1a/GluN2C and GluN1-1a/GluN2D respectively. They also found the glycine EC_{50} values to be 2.1, 0.3, 0.2 and 0.1 μM for the GluN1-1a/GluN2A, GluN1-1a/GluN2B, GluN1-1a/GluN2C and GluN1-1a/GluN2D respectively. From this we can confirm that the receptor pharmacology is largely dependent on the GluN2 subunit forming the NMDAR and that the GluN1-1a/GluN2A subunit combination has the lowest agonist potency (Figure 4). Comparison of single channel behaviour between GluN2A and GluN2B containing NMDARs revealed further differences in receptor pharmacology and kinetics in these receptor subtypes (Erreger et al., 2005). For example, GluN2A receptors responded faster to brief synaptic like pulses of glutamate and proceeded to reach higher open probabilities. Therefore, it can be said that GluN1-1a/GluN2A subunit combinations have faster kinetics of activation that GluN1-1a/GluN2B combinations. The amount of calcium influx is also largely determined by NMDAR kinetics of activation, deactivation, and desensitisation (Johnson and Kotermanski, 2006).

The overall sequence identities between rat and human orthologs of GluN1, GluN2A, GluN2B, GluN2C, and GluN2D are 99.3%, 95.3%, 98.5%, 87.1%, and 95.6%, respectively (Hedegaard et al., 2012). Most of the variation between rat and human orthologs is located within the extracellular amino-terminal domain (ATD) and the

intracellular carboxyl-terminal domain (CTD). Through mutant studies of the ATD, research shows that it plays a regulatory role by influencing many of the differences in receptor pharmacology and kinetics that exist among the NMDAR subtypes (Gielen et al., 2009; Yuan et al., 2009). Only few structural differences are in the ABD and the TMD between the human and rat orthologs, suggesting conservation of key domains that lead to channel gating in response to agonist binding. Since variations between ATDs of rat and human NMDAR subunits exist, there could be inter-species differences in biophysical and pharmacological properties. For example, the GluN2 ATD in both species contributes to the difference in glutamate potency between GluN1-1a/GluN2A and GluN1-1/2D receptors (it is approximately 10-fold lower in GluN1-1a/GluN2A).

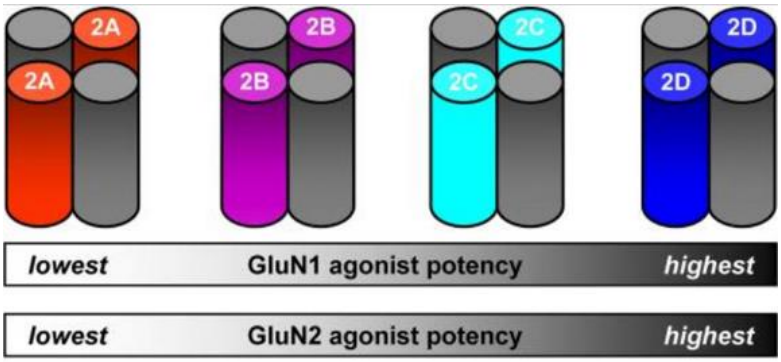

Figure 4. The four different di-heteromeric NMDARs subunit combination, with GluN1 subunits in grey, to show glutamate and glycine potency is lowest at GluN1-1a/GluN2A NMDARs and highest at GluN1-1a/GluN2D NMDARs (Figure taken from (Wyllie et al., 2013))

1.6 Current, failed and developing drug treatments for Alzheimer's Disease

There are currently two types of approved drug treatments that help to relieve symptoms in AD patients. The first type of approved drugs are called cholinesterase inhibitors (Parsons et al., 2013). These work to treat AD by inhibiting the action of acetylcholinesterase (AChE), to increase the levels of ACh available to neurons for synaptic signaling, and therefore improve memory and cognitive deficits. It is also thought that AChE inhibitors could be effective as a treatment due to the role that AChE is believed to have within binding to Aβ to form Aβ plaques, however, this is currently poorly understood (De Ferrari et al., 2001). Donepezil, the first available

AChE inhibitor available in the UK, is FDA approved for use in mild, moderate, and severe Alzheimer disease (Kumar et al., 2021). However, many studies have shown that it brings only small benefits to cognitive functions and activities of daily living, and there is no evidence to suggest that it alters the progression of the disease (Birks and Harvey, 2018; Kumar et al., 2021). Birks and Harvey (2018) carried out clinical trials using mainly doses of 5 and 10 mg/day, some were prescribed 23 mg/day, and they found the benefits of the larger doses were only marginally greater. However, the rates of withdrawal and adverse effects were significantly and unacceptably higher with the 10 and 23 mg/day dose. In contrast, Adlimoghaddam et al. (2018) found that using 23 mg/day of donepezil actually did show statistically significant improvements in cognition, compared to the group that were administered 10 mg/day during their clinical trial studies. However, those receiving higher doses again experienced adverse effects and decided to discontinue their treatment due to this. Thus, confirming that donepezil is not as effective as required, whilst prescribed at a safe dosage that causes no adverse effects, for cognitive and behavioral improvement and certainly has no effect on haltering the disease development.

Rivastigmine, another AChE inhibitor is thought to have great specificity of action and a lower risk of adverse effects (Birks and Evans, 2015). However, the clinical trials carried out by Birks and Evans showed that patients on rivastigmine (6 to 12 mg/day by mouth, or 9.5 mg/day by skin patch) presented with only small benefits to cognitive function and no behavioral changes after 6 months of treatment. Some adverse side effects were still present, however less for those using the patches compared to those taking the oral capsules. Again, there is no evidence to suggest it alters the progression of the disease. A third important AChE inhibitor in circulation for AD treatment is galantamine. A study into the benefits of galantamine highlighted that over a 12 week period, the administration of galantamine (24 mg/day) saw improved cognitive performance (Wilkinson et al., 2001). At lower doses of 18 mg/day, this study saw galantamine to be well tolerated but it still displayed only temporary beneficial cholinergic effects that were typical of other cholinergic treatments. All three discussed cholinesterase inhibitors work in a similar way, but the treatment prescribed to an AD sufferer often depends on the individual as the side effects specifically can be very patient specific. Research continually shows that these drugs do not have the capability to prevent neuronal death or disease

progression and all drugs only slightly relieve the symptoms of AD (Raschetti et al., 2007; Forette and Hauw, 2008). Such research has supported that there are currently no highly effective and side effect free AD treatments, thus leaving much room for further treatment development.

The other approved drug type for AD treatment is NMDAR antagonists. These drugs work by reducing the level of detrimental glutamatergic neurotransmission caused by NMDAR overactivation, thus reducing the amount of neuronal excitotoxicity in AD patients. There are NMDAR antagonists that have been found to be effective during *in vitro* studies, for example MK-801 and ketamine, but they are not yet clinically tolerated and approved (Olivares et al., 2012; Song et al., 2018). Their hindered clinical application is mainly due to the high affinity and long onset time of MK-801 and ketamine at the NMDARs, which causes adverse effects. However, most NMDAR antagonists, including MK-801 and ketamine, also lack in selectivity for overactivated and pathological NMDARs (Ellison, 1995). This is a reoccurring obstacle when developing NMDAR antagonists as drugs that block the regularly functioning NMDARs cause inhibition of physiological activity. Inhibiting physiological NMDARs causes side effects such as psychosis, nausea, amnesia, analgesia but also affects normal synaptic communication, memory function and may potentially result in neuronal cell death (Olivares et al., 2012). Thus, highlighting the necessity for NMDAR antagonist treatments that block only the overactivated NMDARs.

The only NMDAR antagonist in use is memantine, an uncompetitive open channel blocker, licensed for use in moderate and severe AD in Europe and the United States (Olivares et al., 2012). It is also used across Europe and the United States to treat other neurological diseases (Witt et al., 2004). Memantine is the only NMDAR antagonist in use as is the only antagonist found thus far that preferentially blocks higher pathological levels of glutamatergic signaling whilst unaffecting physiological NMDAR activation. It was first synthesised in the 1970s and then found in 1989 to inhibit NMDARs with an IC_{50} of approximately 1 μM (Parsons et al., 2013; Johnson and Kotermanski, 2006). The outcomes of clinical trials of memantine appear to vary slightly across each trial but most reported that memantine has small but beneficial changes to cognition, mood, behaviour, and the ability to perform daily activity in moderate to severe AD patients. Memantine has also been reported many times to

be well tolerated and safe for use as treatment for AD patients and does not appear to have abuse potential (Johnson and Kotermanski, 2006).

Current treatments of memantine are most regularly administered at 20 mg/day (Witt et al., 2004). Farlow et al. (2008) reported that there were minimal adverse effects that occurred from their short- and long-term memantine treatment trials, using 20 mg/day, and any adverse effects that were observed were similar to those experienced from placebo treatment. Kaur (2021) reviewed 10 relevant and completed memantine clinical trials, highlighting that memantine did have positive results on participants with AD by delaying or improving pathological AD symptoms. The most common dose of memantine in the trials was 20 mg/day and at this dosage, minimal adverse effects were observed. Over these 10 trials, it was mostly moderate to severe AD patients used and the impact of memantine in mild to moderate patients remains unknown (Olivares et al., 2012). However, overall memantine is still yet to show any signs of high levels of decrease in clinical deterioration and does not delay disease development. Therefore, the search for a more potent drug with similar actions to memantine, but that provides greater benefits to the patient, is still ongoing.

There is also an increased therapeutic benefit to using combination therapy of memantine alongside an AChE inhibitor for the treatment of AD (Parsons et al., 2013). As discussed, both drug types have presented as successful monotherapies and research shows there is more benefit to using them as combined therapies to target the cholinergic and glutamatergic systems at once. There are also interrelations between the cholinergic and glutamatergic pathways that affect the regions of the brain that control learning and memory, making combination therapy an even more appropriate treatment path. Glutamatergic neurons in the amygdala, reticular formation, hippocampus, and cerebral cortex make synaptic connections with cholinergic neurons located in the medial septum, diagonal band of Broca and the nucleus basalis of Meynert. These cholinergic neurones then innervate the neocortex and hippocampus. Excessive activation of NMDARs has been implicated in processes underlying the degeneration of cholinergic cells in AD. For example, neuronal degeneration caused by direct injection of NMDA into the rat basal forebrain leads to reduced levels of ChAT activity in the cortex. Therefore, it seems

that cholinergic neurones are vulnerable to the hyperactivity of the NMDARs. Thus, supporting that the use of both drugs combined has good potential to treat AD. Previous research using animal models has shown that the combined use of memantine and AChE inhibitors achieved greater improvements in memory in comparison to individual treatments. The effect of memantine and donepezil as combined treatments was examined in young and old triple-transgenic mice that were exhibiting cognitive impairments and high levels of amyloid beta plaques and NFTs in the brain (LaFerla et al., 2009). The mice were treated with the two drugs separately and combined to compare, and the memantine-donepezil combination significantly improved the spatial memory in all of the mice. The results of this study suggested that the combination therapy was effective in improving cognitive performance in the young and old mice who demonstrated AD-like pathology.

The method of combining treatments has also been investigated multiple times in human clinical trials. In one randomised, double-blind controlled study in 404 patients with moderate to severe AD, treatment with memantine and donepezil produced significant benefits across cognitive, functional, behavioural, and global domains, when compared with donepezil monotherapy (Tariot et al., 2004). However, in contrast, a study using 433 patients with mild to moderate AD demonstrated that the combined therapy was not found to be significantly better than the AChE inhibitors monotherapy (Porsteinsson et al., 2008). Further research to address the differences in these clinical trial results excluded the data collected for patients suffering from mild AD (Atri et al., 2013). Here, it was found that there were significant benefits of the combination treatment compared to donepezil monotherapy for patients with moderate to severe AD. Therefore, supporting that the combined treatment does have significant effects to patient cognition but also supports that there is still a gap within treatment for mild AD patients. In summary, preclinical data has confirmed that the combination of memantine and an AChE inhibitor may be a useful approach for the management of AD.

Innovative research is currently exploring a new therapy that combines multiple pathological targets into one drug treatment. Rosini et al. (2008) presented multiple compounds that targeted both AChE and NMDAR inhibition and they found that a compound called carbacrine was able to significantly inhibit the AChE activity in the

nanomolar range and was found to antagonise NMDARs. Interestingly, they also found carbacrine to block *in vitro* Aβ self-aggregation and aggregation mediated by AChE. This highlighted a potential direction for AD therapies within multi-target-directed ligands and from this, further work into other compounds like this continued. Rosini et al. (2013) continued such research and concentrated on the antihistamine drug called dimebon that showed the ability to simultaneously inhibit NMDARs and AChE. Dimebon however presented with clinical failure which was attributed to its low *in vitro* activity (IC_{50} 42 μM for AChE and 10-70 μM for NMDARs). Therefore, Rosini et al manipulated the structure of dimebon to synthesise 5 compounds by connecting the γ-carboline moieties of dimebon with variable-length polymethylene spacers and heteroatom or aromatic linkers. In doing so they found that all 5 compounds showed inhibition of both AChE and NMDARs. These positive results highlight that the route of multi-target-directed ligands may be successful in the development of AD treatment therapies.

1.7 Memantine

Memantine (1-amino-3,5-dimethyladamantane) is an amino alkyl cyclohexane derivate (Figure 5) and importantly, it binds to NMDARs with moderate affinity and voltage dependency (Olivares et al., 2012). This therefore means that memantine is relatively ineffective at blocking low levels of NMDAR activity that is associated with physiological neuron function and that memantine can moderate levels of prolonged stimulation that occurs under pathological conditions (Parsons et al., 2013). When a physiological signal arrives and increases the glutamate concentrations in the synapse, the memantine dissociates from the receptor to allow normal physiological neurotransmission to proceed (Figure 6). Memantine is an open channel blocker as it requires the NMDAR to be already activated and open for it to bind in the channel pore. Once tightly bound, the memantine inhibits the excessively open NMDAR to prevent excessive influx of Ca^{2+} ions into the neurone.

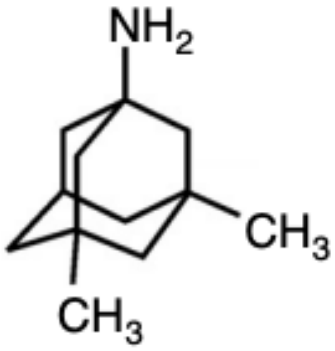

Figure 5. Structure of memantine (Johnson et al., 2015)

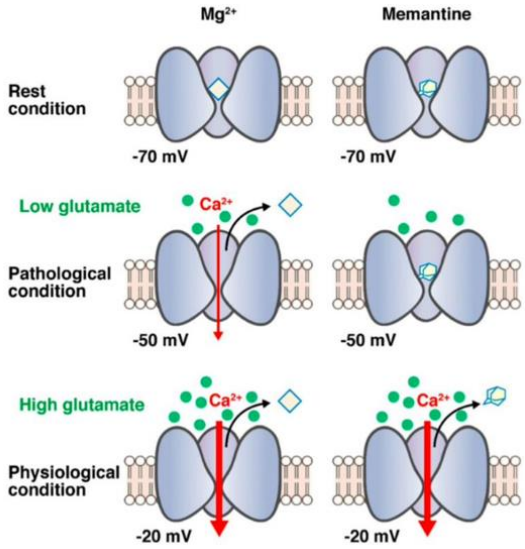

Figure 6. Figure showing the differences between Mg^{2+} ion block and memantine block of NMDAR during physiological and pathological periods. Highlights that memantine remains present in ion channel under pathological levels of glutamate (Figure taken from (Kikuchi, 2020))

To understand memantine's therapeutic action it is important to recognise its moderate affinity and rapid off-rate kinetics at the level of NMDARs (Olivares et al., 2012). The fast off-rate means memantine should not, and has been found to not, overly accumulate in the NMDAR channels. This contributes to memantine's ability to avoid affecting normal physiological synaptic transmission and receptor function. The rapid off-rate and moderate affinity, shown by the IC_{50} being around 1 μM, also underpins the tolerability and low adverse effects profile previously discussed for memantine. In terms of different receptor subtypes, research shows that memantine has a higher potency to GluN1-1a/GluN2D and GluN1-1a/GluN2C responses compared to responses mediated by GluN1-1a/GluN2A and GluN1-1a/GluN2B NMDARs (Kotermanski and Johnson, 2009). This suggests that differences in the

structure and combination of NMDAR subunits, can result in differences in the potency of memantine (Parsons et al., 2013). Memantine is also often referred to as a “better magnesium” as it has a slower unblocking rate, slightly higher affinity, and moderate voltage dependency. The voltage dependent profile underpins that during normal synaptic activity, where there is strong membrane depolarisation, memantine is unable to bind or accumulate in the channels (Parsons et al., 2013). Therefore, physiological synaptic activity continues, and ion permeation is permitted. However, as mentioned, memantine inhibits ion permeation under weak depolarisation, which is often caused by pathological leakage of glutamate into the synapse or remaining glutamate from pathologically reduced uptake, and therefore there is prolonged activation/opening of the receptors in which memantine becomes a highly effective channel blocker.

Understanding the mechanism by which memantine and other NMDAR antagonists bind to receptors helps research working towards finding the most effective and safe NMDAR antagonist. Memantine possess a three ring (adamantane) structure with a bridgehead amine ($-NH_2$) that carries a positive charge (Figure 5). The positively charged amine group binds at or near the Mg^{2+} ion binding site within the NMDAR channel (Olivares et al., 2012). More specifically, memantine is known to bind through interactions of the $-NH_2$ and the N-site asparagine residues in M2 region of the GluN1 subunits (Chen and Lipton, 2005). However, the N and N+1 site asparagine residue in the M2 region of the GluN2 subunits also appear to produce strong electrostatic interactions with memantine (Figure 7). The asparagine residues are found at the tip of the subunit pore loop (Limapichat et al., 2013). Mutagenesis studies have recently confirmed that the sites at which Mg^{2+} ions and memantine bind to overlap. This was demonstrated by showing that mutations of the asparagine residues in the M2 regions of GluN1 and GluN2 subunits, which are critical for Mg^{2+} ion block, also strongly affected the memantine block (Kotermanski et al., 2009). During this study, the IC_{50} of memantine (at V_h = -66 mV), on the GluN1-1a (N616Q)/GluN2A mutant NMDARs, increased from 1.25 μM, recorded from GluN1-1a/GluN2A wild type receptors, to 2.88 μM.

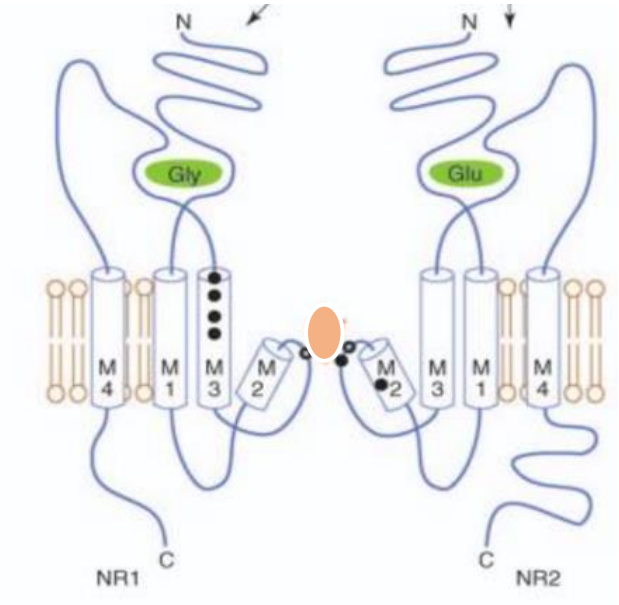

Figure 7. Figure showing NMDAR with one GluN1 subunit and one GluN2 subunit with their respective agonists (green). In channel pore there is the memantine block (orange) at the M2 region (Figure taken from (Johnson and Kotermanski, 2006))

When looking more specifically at the IC_{50} values recorded for NMDAR inhibition by memantine, a range of around 0.7-1.7 μM trends at a holding potential of around -60 mV (Glasgow et al., 2017; Chen and Lipton, 2005; Kotermanski and Johnson, 2009; Gilling et al., 2009). Research by Chen and Lipton (2005) showed the IC_{50} value of memantine inhibition, at -60 mV holding potential, on GluN1-1a/GluN2A NMDARs, to be 0.9 μM. Glasgow et al. (2017) used whole patch clamp recordings to test the inhibitory effects of memantine on NMDARs, finding the IC_{50} to be 1.33 μM (V_h = -65 mV). Interestingly, research conducted by Aracava et al. (2005) showed memantine to exert inhibitory effects on the cholinergic system, alongside the glutamatergic system. Whilst testing on primary rat hippocampal neurones, using patch clamp electrophysiology, memantine caused a concentration-dependent reduction of the whole-cell currents evoked by the α7-nAChRs agonist choline (10 mM); at -60 mV the IC_{50} value was recorded as 0.34 μM at α7-nAChRs. This level of blockade at therapeutically tolerant concentrations could inhibit neurotransmission during early stages of the disease when functioning cholinergic neurones are still available and henceforth, memantine is currently only used in later stages of the disease (Anand et al., 2014). Memantine also showed significant voltage dependency when inhibiting α7-nAChRs in this study. Findings by Aracava et al. (2005) are supported by another study conducted by Maskell et al. (2003). They found, through two-electrode voltage-

clamp (TEVC) recordings of human α7-nAChRs expressed in *X. laevis* oocytes, that memantine does inhibit α7-nAChRs in a voltage dependent manner. More specifically there was inhibition of ACh-induced inward currents observed (IC_{50} 5 μM at V_h -75 mV). The significant difference between the IC_{50} values for the α7-nAChRs might result from experimental differences (recombinant human receptors expressed in *X. laevis* oocytes versus receptors in rat primary hippocampal neurones) or the inclusion of subunits other than α7 in the rat receptors (Johnson and Kotermanski, 2006). These multitarget properties of memantine are an interesting property to look for elsewhere in other compounds that show potential for AD therapeutic treatments.

1.8 Natural NMDAR antagonists

Upon research into uncompetitive open channel antagonists like memantine, several natural NMDAR antagonists were discovered. One natural antagonist, called Argiotoxin-636 (ArgTX-636), was found in spider venom from *Argiope lobata* species (Poulsen et al., 2013). ArgTX-636 was confirmed to be an open channel blocker of NMDARs and found to be extremely potent with affinities in the nanomolar range (Poulsen et al., 2015). Brackley et al. (1993) found ArgTX-636 to inhibit rat NMDAR expressed in *X. laevis* oocytes, with an IC_{50} value of 0.04 μM when using NMDA-induced currents. Further work explored a polyamine-containing toxin called philathotoxin-343 (PhTX-343), which is isolated from the Egyptian digger wasp and is structurally related to ArgTX-636. Research showed PhTX-343 to also exhibit high selectivity for NMDARs. Brackley et al. (1993) found the IC_{50} value of antagonism of NMDA-induced currents to be 2.5 μM, and Mellor et al. (2003) found the value of antagonism of NMDA-induced currents to be 2.01 μM when using PhTX-343. Further research found that antagonism of NMDAR responses by PhTX-343 and ArgTX-636 are reversible, non-competitive, and partly voltage-dependent. The abundance of research into natural NMDAR antagonists led to the interest in ladybird toxins and alkaloids.

1.9 Ladybird alkaloids and their defence systems

Ladybird beetles are from the family Coccinellidae. They are found worldwide and are extremely specie rich as they have over 6000 species (Seago et al., 2011). They are yellow, orange, or red in colour with black spots on their wing covers, which are

called elytra. The colour and spot variation of individual ladybirds is greatly varied and are an aposematic warning of toxicity. There is a documented correlation between the colouration and spot markings of the elytra, with the concentration of alkaloids within; those with brightly coloured and more marked elytra appear to have higher toxic concentrations (Bezzerides et al., 2007). Different species of ladybirds possess an extensive range of alkaloid-based compounds that are released from their tibiofemoral joints when the ladybirds are exposed to threat. The haemolymph appears as an orange-yellow liquid.

Historically, the Harlequin ladybird *Harmonia axyridis (H. axyridis),* which is a native species to central Asia, was introduced to many countries as a biological control agent (Vilcinskas et al., 2013; Roy and Wajnberg, 2008). The aim was to use the species to prey on aphids and other insect pests that were present in these countries. However, *H. axyridis* were able to outcompete native ladybird species and it turned into an invasion. This was attributed to *H. axyridis* having a high tolerance for other species' alkaloids whilst being able to use their own toxic alkaloid levels to protect themselves (Sloggett and Davis, 2010). It is thought that *H. axyridis* can modify and store different alkaloids to enable this successful predation and survival against other ladybird beetles. To also protect them from other species, they have adapted a chemical defence system for their eggs. The *H. axyridis* eggs synthesise alkaloids internally, causing the egg to become toxic and as a result the surface of the egg is often coated in a mixture of toxic alkaloids. This internal and external toxicity of the egg creates an unpleasant tastes and means that they are generally protected from predators (Magro et al., 2018). It was also found that in comparison to the native species, the *H. axyridis* haemolymph contained strong antibacterial activity (Vilcinskas et al., 2013). This activity was attributed to harmonine; a secondary metabolite that accumulates at high levels in the haemolymph.

1.10 Harmonine

Harmonine is an acyclic amine, and it appears as a brownish oil when extracted from ladybirds and isolated from the other alkaloids in the haemolymph (Figure 8). The role of harmonine in the *H. axyridis'* antimicrobial properties was observed through monitoring the inhibitory effects of harmonine on mycobacterial growth. Harmonine was documented to have large inhibition zones when grown on *E. coli* containing

agar, compared to haemolymph from other ladybird species which presented no growth inhibition zones. During such research into harmonine's antimicrobial properties, harmonine was found to reduce AChE activity. Alam et al. (2002) confirmed slight inhibitory actions of AChE by harmonine. Their research involved using *H. axyridis* alkaloid extract (HAE), as harmonine is difficult to individually extract. HAE is believed to be 90% harmonine as shown using Gas chromatography – Mass Spectrometry analysis (Figure 9). The Gas chromatography – Mass Spectrometry analysis produced a chromatogram (C) showing multiple compounds present in the HAE, the predominant compound being harmonine. As aforementioned, AChE is a therapeutic target for AD therapeutic treatment, so these discoveries of HAE inhibitory action opened potential for the use of HAE as an AD treatment. Similar research by scientists continued to confirm the inhibitory action of HAE on nAChR. Richards (2011) used whole-cell patch clamp electrophysiology to demonstrate that HAE had potent antagonistic effects on nAChR in human muscle TE671 cells and locust neurons. Here HAE, at V_h = -50mV, had IC_{50} values of 2.12 μg/ml (7.5 μM).

Further research by Patel et al. (2020) found HAE to be voltage dependent in its inhibitory action, thus similar to the voltage dependent action of memantine. As discussed, compounds like memantine, that target nAChRs, can also potentially target NMDARs (Zhou & Sheng 2013a). Following this knowledge, HAE was found to inhibit GluN1-1a/GluN2A NMDARs with an IC_{50} of 0.179 μg/mL at Vh = -75 mV (Patel, 2017). Thus, suggesting that HAE has multitarget properties yet to be further understood. More recent research by Kaur (2021) found HAE to inhibit rat GluN1-1a/GluN2A NMDARs at an IC_{50} value of 1.11 μg/mL at V_h = -75mV (~3.9 μM). Therefore, research suggests that HAE may be able to offer some similar therapeutic treatment for AD through inhibition of NMDARs as seen for memantine with the added benefit of AChE inhibition like donepezil, rivastigmine and galantamine.

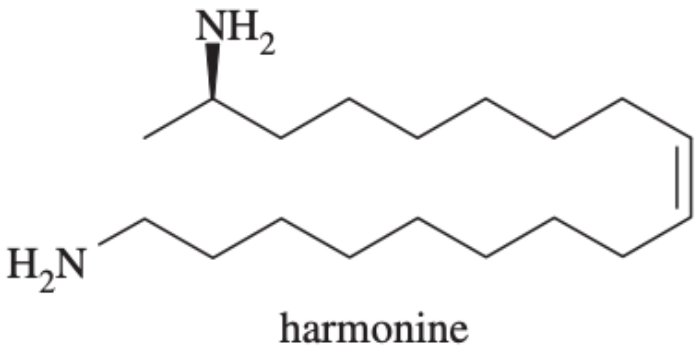

Figure 8. Chemical structure of harmonine (Röhrich et al., 2012)

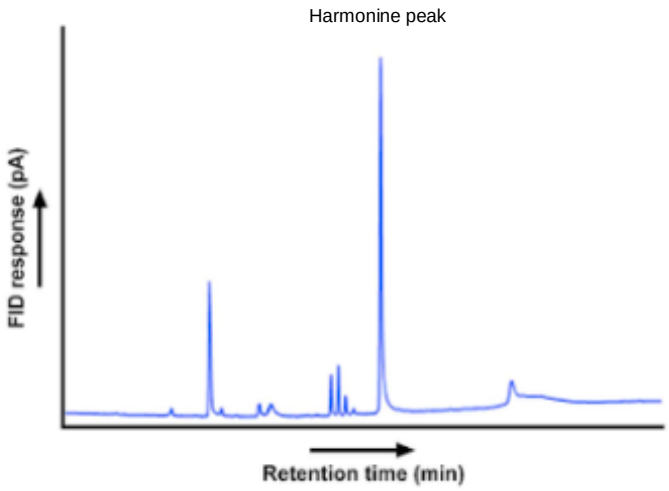

Figure 9. Gas-chromatography – Mass Spectrometry analysis produced a chromatogram showing multiple compounds present in HAE including the main alkaloid harmonine (labelled above) (Figure taken from Patel, 2020)

1.11 Potential use of Harmonine analogues

In accordance with the antagonistic effects of HAE on NMDARs, harmonine analogues may show further success in inhibiting NMDARs. There is no research at present using harmonine analogues, however, investigating HAE analogue effects is a beneficial approach to potentially accelerate drug treatment development for AD through NMDAR antagonists. Also, using harmonine analogues to investigate their inhibitory effects on NMDAR is a way to confirm that the inhibitory effects observed when using HAE as an antagonist of NMDARs is from the action of the 90% harmonine compound.

1.12 Aims and Objectives

The main aim of this study is to investigate the antagonistic effects of HAE and an analogue of harmonine on NMDARs in comparison to memantine. These comparisons will be drawn using electrophysiology two-electrode voltage clamp (TEVC) electrophysiology to test effects of the antagonists on human GluN1-1a/GluN2A subunit combinations of NMDARs when expressed in *Xenopus laevis* oocytes. Research thus far for HAE has been conducted primarily on rat clones and therefore it is important to confirm and show the actions of these compounds on human NMDARs.

2 Methods

2.1 Chemical reagents and plasmids

NMDA was from Acros Organics and memantine was from Apexbio. cDNA clones of human NMDARs (GluN1-1a and GluN2A) were sourced from GenScript. The accession numbers for the clones were NM_007327.4 and NM_001134407.3 for GluN1-1a and GluN2A respectively. The HAE was acquired from the laboratory of Dr Mike Birkett, Rothamsted Research, and the harmonine analogue used was provided by Dr Alex Bissember, University of Tasmania, Tasmania. The harmonine analogue (Figure 13) was about 95% pure with the rest being the trans-isomer, MW 282.2, $C_{18}H_{38}N_2$ and will be referred to as ‘harmonine analogue’ within this paper. Unless otherwise stated, all other compounds and reagents were sourced from Sigma Aldrich.

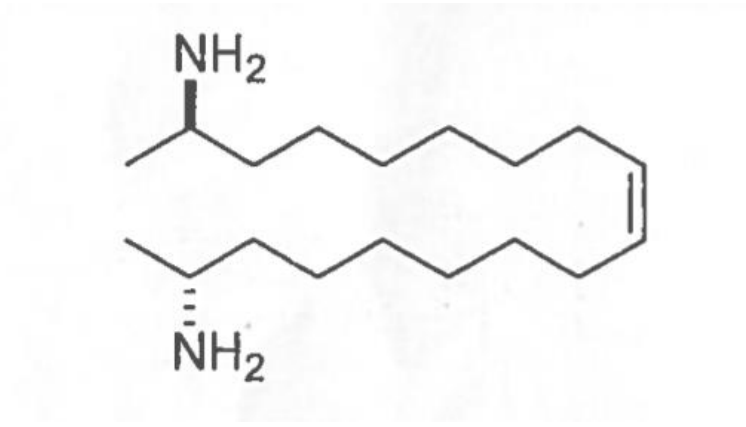

Figure 13. Skeletal formula of harmonine analogue, $C_{18}H_{38}N_2$, MW 282.2.

2.2 Transformation of plasmid DNA into XL-10 Gold supercompetent *E. coli* cells using heat shock technique

Modified Lysogeny broth (LB), LB agar and SOC medium were made prior to the transformation steps in this method. The LB broth consisted of 10 g/L NaCl (96mM), 10 g/L tryptone and 5 g/L yeast extract, pH 7, autoclaved and stored for up to 1 month at 4°C. The LB agar was the same composition as LB with the addition of 17 g/L agarose before autoclaving and 50 mg/L ampicillin after. Once the LB agar was poured into petri dishes and set, the agar plates were stored for up to 1 month at 4°C. The SOC medium was made by the addition of 18.016 mg glucose per 10 mL (10 mM) of LB, pH 7.5, autoclaved and stored at 4°C for 1 month.

Transformation of the plasmid DNAs encoding human NMDAR subtypes GluN1-1a and GluN2A (GenScript) was performed using XL-10 Gold supercompetent *E. coli* cells and the heat shock technique. During the method, an optimised protocol was established. To begin, the supercompetent XL-10 Gold cells were removed from the -80°C freezer and thawed on ice. Within a fume cupboard, 200 µL of XL10-Gold supercompetent cells were added to an Eppendorf tube with 2 µL of 2-mercaptoethanol. This was agitated and then chilled on ice for 10 minutes; swirling every 2 minutes. Subsequently 2 µL of the DNA plasmid of choice (GluN1-1a or GluN2A) was added to the Eppendorf tube and incubated on ice for 30 minutes; swirling every 10 minutes. The Eppendorf tube was then heated at 42°C for 45 seconds in a water bath, before moving cells back to ice for 2 minutes. 950 µL of preheated (42°C) SOC was added to the tube and incubated for 1 hour at 37°C with shaking at 250 xg. After 1 hour, 250 µL of the cells were added to an LB agar plate under aseptic conditions and then incubated at 37°C for between 15-20 hours 24 hours.

2.3 Isolation of DNA from recombinant *E. coli* cultures

After the 24 hours, a single colony was collected using a sterile pipette tip and inoculated in 5 mL of LB broth with 100 µg/mL ampicillin, then left overnight at 37°C under vigorous shaking (250 xg). This started the colony growth for the isolation of DNA from the recombinant *E. coli* cultures. The isolation was carried out using established protocol steps from the GenElute™ Plasmid Miniprep Kit (70 prep

package) (SIGMA). Before the process, two solutions were prepared. The Miniprep Kit contains a tube of RNaseA, and the tube was centrifuged before adding 78 μL to the resuspension solution provided (then stored at 4°C). The wash solution was created by dilution of the wash solution with 100 mL of 100% ethanol. After each use of the wash solution, the bottle was tightly capped to ensure there is no evaporation of ethanol.

Once the solutions were made, protocol steps for isolation were as follows and were carried out at room temperature. Firstly, the recombinant *E. coli* culture was transferred to an Eppendorf tube, 1500 μL at a time, and the tubes were spun in a centrifuge (5417R Eppendorf Centrifuge Machine) at 14,000 xg for 1 minute to pellet the cells. The supernatant was discarded, and this step was repeated until all the solution was used. Next, the bacterial pellet was resuspended with 200 μL of resuspension solution until homogenous. The resuspended cells were then lysed by adding 200 μL of the lysis solution, the contents of Eppendorf were then immediately mixed by gentle inversion (6-8 times) until the mixture became clear and viscous. After 4 minutes of cells left in lysis solution, the cell debris was precipitated by adding 350 μL of the neutralisation/binding solution. The tube was inverted 4-6 times and then cell debris was pelleted by centrifuging at 14,000 xg for 10 minutes. Next, a GenElute Miniprep binding column was inserted into a microcentrifuge tube and 500 μL of column preparation solution was added to the column. The binding column was centrifuged at 14,000 xg for 1 minute then the flow through liquid discarded. The cleared lysate with the added neutralisation/binding solution was transferred to a prepared column and centrifuged at 14,000 xg for 1 minute, and then the flow through liquid discarded. 750 μL of the diluted wash solution was then added to the column, centrifuge at 14000 xg for 1 minute, flow through liquid discarded and the tube was centrifuged again with the same setting for 2 minutes. The binding column was moved to a fresh collection tube and 100 μL of Elution Solution was added to the column, centrifuged at 14,000 xg for 1 minute and the DNA was then present in the eluate.

Once the isolation of DNA from the recombinant *E. coli* cultures was complete, the concentration of the DNA was checked using a Nanodrop spectrophotometer

(Thermo Scientific), aiming for 200 ng/µL and a contamination of around 1.7-2.0. Once the concentration was confirmed to be in a good range, the DNA was ready for immediate use or storage at -20°C.

2.4 DNA restriction digest

To transcribe RNA from the cDNA template it was first necessary to linearise the plasmid DNA using restriction enzymes. NotI restriction enzymes was used for both GluN1-1a and GluN2A subunits as the human subunit DNA clones were inserted into the pcDNA3.1 (+) plasmid just upstream of this restriction site. The restriction digestion reaction involved adding 1 µL of the restriction enzyme, 2 µg of the relevant subunit plasmid DNA and 5 µL of 10x NEBbuffer to a 1.5 mL Eppendorf tube. The total volume of the tube was then made up to 50 µL with dH_20. The tube was then placed into a 37°C water bath for 2 hours. After two hours, 5 µL of ammonium acetate stop solution, from a mMESSAGE mMACHINE T7 kit (Thermo Fisher), and 100 µL ice cold 100% ethanol was added to the mixture and kept at -20°C overnight to completely terminate the restriction digestion reaction. The next day, the mixture was spun at 14,000 xg, 4°C for 15 minutes. Following this, the supernatant was decanted, and tube was span again under same conditions for 30 seconds. The supernatant was again decanted, and the tube was then placed open in a 50°C water bath for approximately 5 minutes to dry the DNA pellet. After drying, the DNA pellet was resuspended in 15 µL of nuclease-free water and then placed back into a 50°C water bath with the tube closed for a further 5 minutes. The tubes were then spun at 14,000 xg for 30 seconds before the Nanodrop spectrophotometer (Thermo Scientific) was used to determine the linearised pDNA concentration.

2.5 Agarose gel electrophoresis

To ensure that the linearisation of the plasmid DNA occurred, and the restriction enzymes made only one cut at the required place, agarose gel electrophoresis was used to visualise the linearised pDNA and compare it to the plasmid DNA. 5 X Tris-Borate-EDTA (TBE) stock solution was prepared using 54 g Tris, 27.5 g Boric Acid, 20 mL 0.5 M EDTA, pH 8, in 1 L dH_20. The TBE stock solution was then diluted to 1 X TBE using distilled water. 1 g of agarose powder was then added to 100 mL of 1 X TBE and dissolved by interval heating in the microwave until the mixture began to

boil. Once the mixture was cool enough to handle, 1 µL of 1% ethidium bromide was added, swirled, and then poured into the prepared gel electrophoresis mould and left to solidify. The mould was then placed into the gel electrophoresis kit (Bio-Rad) and the tank was filled with 1 X TBE until the mould was fully immersed. 1 µL of the DNA samples and for the 1 kb DNA ladder (New England Biolabs) were mixed with 1 X loading dye before loading into the wells. The gel was run at 150 V for 1 hour and the DNA bands were then visualised using iBright 750 (Invitrogen by Thermo Fisher Scientific). Examples of the linearised pDNA in comparison to the plasmid DNA are shown in the gels in Figure 10.

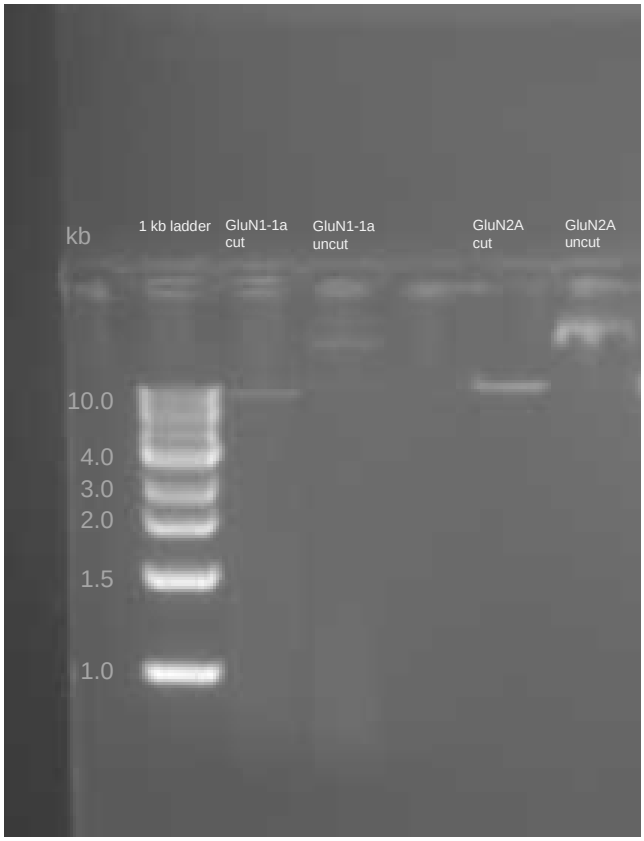

Figure 10. Image taken from iBright 750 (Invitrogen by Thermo Fisher Scientific) of agarose gel of plasmid (uncut) and linearised (cut) pDNA of GluN1-1a and GluN2A NMDAR subunits. From left to right on image: 1 kb of DNA ladder, linearised GluN1-1a, uncut GluN1-1a, linearised GluN2A and uncut GluN2A. Ladder labelled on the left side of image in grey. The linearised GluN1-1a and GluN2A were their expected sizes, 10,859 bp and 9,821 bp, respectively.

2.6 mRNA transcription

mRNA transcription was carried out using the mMESSAGE mMACHINE T7 kit (Thermo Fisher) for the GluN1-1a and Glu2A subunits because the genes were inserted into a pcDNA3.1 (+) with T7 promoter. Using the kit materials, 0.1-1 µg of linearised pDNA was added to 10 µL NTP/CAP 2X, 2 µL reaction buffer 10X and 2 µl enzyme mix in a 1.5 mL Eppendorf tube. The volume was made up to 20 µL using nuclease-free water, forming the reaction assembly. The reaction assembly was flicked to set at the bottom before incubating in a 37°C water bath for 2 hours. Proceeding the 2 hours, the reaction was terminated, and the RNA was recovered, by adding 30 µL lithium chloride precipitation solution and 30 µL nuclease free water. This was frozen overnight at -20°C to ensure complete termination of the reaction. Next day, the RNA was centrifuged at 14,000 xg for 30 minutes at 4°C. The supernatant was then aspirated, and the RNA pellet was washed with 1 mL of 70% ethanol and spun again for 30 minutes. The supernatant was decanted and spun for a following 30 seconds. The pellet was then dried by placing the tubes open in a 50°C water bath for approximately 5 minutes. The pellet was then resuspended in 15 µL of nuclease free water. The concentration of the RNA was then measured using the Nanodrop Spectrophotometer. A desired concentration of 200 ng/µL and a contamination of around 2.0-2.2 were aimed for. The RNA aliquoted into 5 µL amounts and stored at -80°C until used for oocyte injection.

2.7 *Xenopus laevis* oocyte preparation and RNA microinjection

Xenopus laevis oocytes were acquired from the European Xenopus Resource Centre, University of Portsmouth, Portsmouth, UK (Figure 11a). On arrival of the *X. laevis* oocytes, they were treated with 2.5 mg/mL of collagenase (*Clostridium histolyticum* type 1A, Sigma) in 10 mL of Ca^{2+}-free Barth's gentamicin theophylline pyruvate (GTP) Solution, for approximately 1 hour at 18°C, to breakdown the connective tissue and outer follicular tissue layer that surrounds each oocyte cell. The Ca^{2+}-free GTP contained 5.61 g/L NaCl (96 mM), 0.15 g/L KCl (2 mM), 1.19 g/L HEPES (5 mM), 0.275 g/L pyruvic acid (2.5 mM) and 0.09 g/L theophylline (0.5 mM), pH 7.5 with NaOH, and autoclaved before use. Gentamicin (0.05 mg/mL) was added after the autoclaving. After the hour, the oocytes were washed with Ca^{2+}-free GTP approximately 5 times and then the cells were incubated in petri dishes in GTP, until

use, at 18°C. GTP has the same composition as Ca^{2+}-free GTP with the inclusion of 1.8 mM $CaCl_2$ (1 M), also at pH 7.5.

After washing and ensuring the outer follicular layer of each cell was fully removed using a microscope, healthy oocytes were selected ready for RNA injection of NMDARs (Figure 11b). 1.5 µL of GluN1-1a and GluN2A RNA subtypes (ratio 1:1) with concentrations between 60-200 ng/µL were pipetted onto a petri dish and then filled into a glass injecting pipette. The injecting pipette was pulled from borosilicate glass capillary tubes (World Precision Instruments, 504949), pulled using a Sutter P-90 pipette puller, and the end of each pipette was carefully broken to about 25 µm using a pair of forceps. The pipettes were backfilled with paraffin oil to create hydraulic pressure before being mounted onto a Nanolitre 2010 injector (World Precision Instruments, Inc.), ready for the uptake of the RNA, ensuring no bubbles were drawn into the injecting pipette. Each oocyte cell was injected with 50 nL of the combined RNA solution. Each injected oocyte was incubated in fresh and sterile GTP in 24-well plates for 3-4 days at 18°C to express the NMDARs ready for electrophysiological recordings.

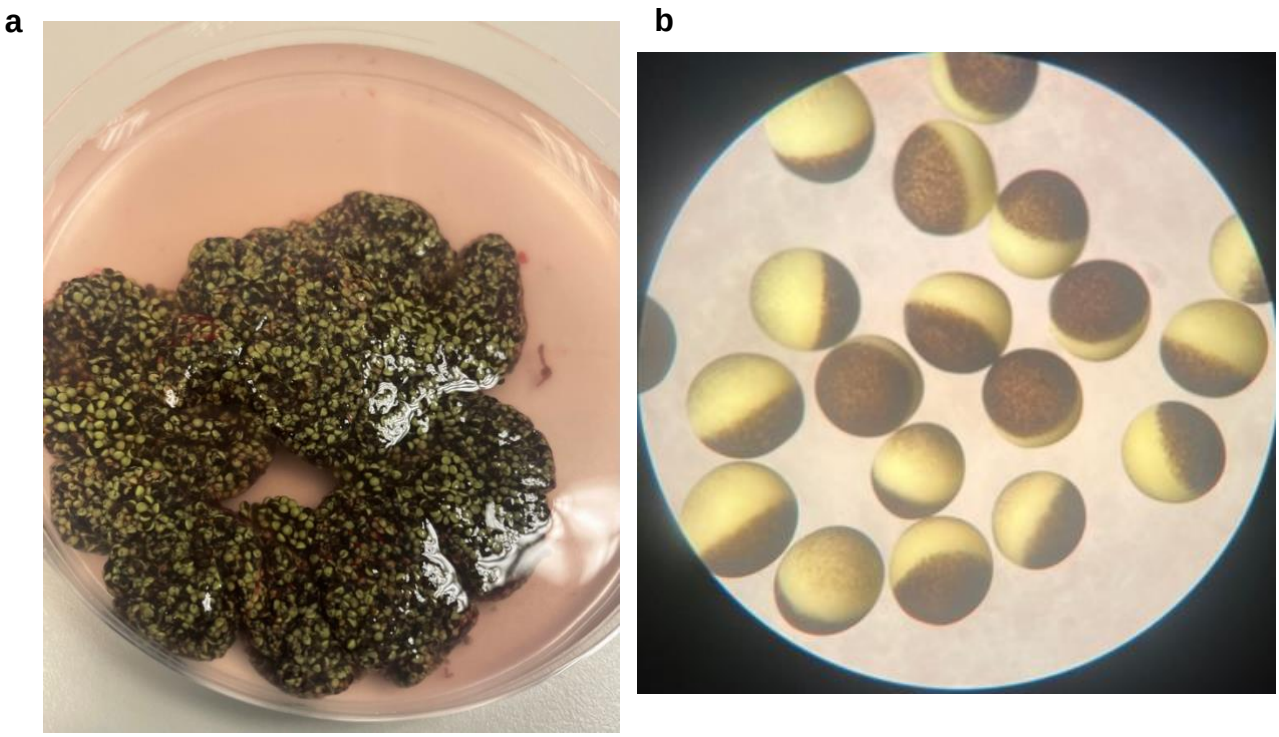

Figure 11. a) Image of *X. laevis* oocyte cells on arrival before collagenase treatment. b) Microscope image of healthy and follicular layer peeled *X. laevis* oocyte cells

2.8 Whole alkaloid extraction

HAE used was produced externally as follows. Adult *H. axyridis* ladybirds were collected from the grounds of the University of Nottingham and Rothamsted Research (Harpenden, Hertfordshire), then stored at -20°C until use. The beetles (ca. 5000 weighing ca. 187 g) were then frozen in liquid nitrogen before being crushed and soaked in methanol (2 x 250 mL) for 24 hours at room temperature. The mixture was then filtered using filter paper (Grade 4, Whatman), combined and dried using a rotary evaporator (BUCHI, Switzerland). The residue from drying (ca. 8 g) was then used for acid-base extraction using 1 M HCL (50 mL) and diethyl ether (3 × 20 mL) to remove lipoidal material, followed by adjustment to ca. pH 10–12 using NaOH (2 M), at room temperature. This was then extracted using dichloromethane (3 x 20 mL) and then washed with saturated NaCl solution. Next it was dried using anhydrous $MgSO_4$ and evaporated to then yield a residue (ca. 450mg). The residue was re-dissolved in di-chloromethane and aliquots of HAE residue (300 µg and 500 µg) were measured for storage in glass ampoules sealed under nitrogen.

2.9 Two-electrode voltage-clamp electrophysiology

All electrophysiological recordings were obtained from NMDAR expressing oocytes by TEVC using an Axoclamp 2A voltage clamp amplifier (Axon instruments, USA). To use the TEVC, an oocyte was transferred to the recording bath using a plastic Pasteur pipette and the bath was continually perfused with modified Xenopus ringer solution (MXR solution). MXR contained 5.6 g/L NaCl (95 mM), 0.15 g/L KCl (2 mM), 2 mL/L of 1 M $CaCl_2$ (2 mM), 1.19 g/L HEPES (5 mM), pH 7.5. Microelectrodes for all TEVC recordings were pulled from borosilicate glass capillaries (GC150TF-10, Harvard Apparatus) using a P-90 Flaming Brown micropipette puller (Sutter instrument company). The microelectrodes were 75% filled with 3 M KCl and checked for a resistance between 0.5 to 2 MΩ.

2.10 TEVC of *X. laevis* oocyte cells

After transfer of an oocyte cell, the TEVC microelectrodes were inserted into the cells as shown in Figure 12 and the holding potential (V_h) was set at -75 mV. The microelectrodes were inserted using the micro-positioners and pushed in once they were resting on the external part of the oocyte, as shown in Figure 12b. Successful

insertion of the microelectrodes was confirmed by the membrane potential of the oocyte reading between -20 and -60 mV on the Axoclamp, 2A. Output currents from the Axoclamp, 2A were transferred using a PCI-6221 A/D converter (National Instrument Corp., US) to a PC and WinEDR software (Dr John Dempster, Institute of Pharmacy & Biomedical Sciences, University of Strathclyde, UK) was used for recording. This technology for recording responses was used consistently throughout all TEVC use in this study. Once voltage-clamped, a solution containing 10^{-4} M NMDA plus 10^{-5} M glycine was applied to the oocyte via an 8-valve perfusion system (Automate Valvelink 8) to test for NMDAR expression. Control experiments were conducted with uninjected oocytes to show that all data collected from the next stages was due to NMDAR expression and no alternate interactions between the wild type oocytes and the agonists.

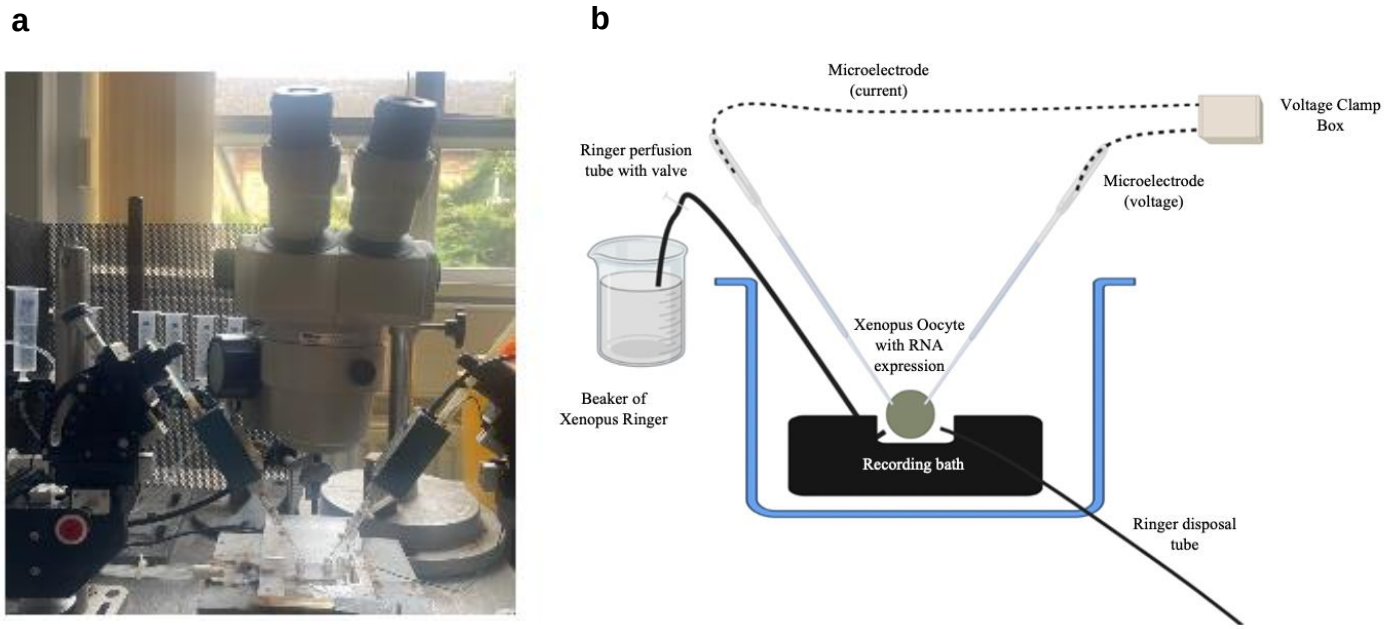

Figure 12. a) Image of TEVC set up used b) Simplified image of Figure 2a to explain set up of *X. laevis* oocyte TEVC recording

2.11 TEVC memantine antagonist recordings

Memantine 10^{-2} M stock solution was made in MXR and stored at -20°C until use. For use, the stock solution was made into serial dilutions, in NMDA (10^{-4} M) and glycine (10^{-5} M) agonist solution, from 10^{-4} M down to 10^{-8} M. Firstly, NMDA (10^{-4} M)

and glycine (10^{-5} M) agonist solution was applied until the response achieved a steady state (plateau), then the memantine dilutions were consecutively co-applied, starting with the lowest concentration, and progressing up to the highest, by switching to the next concentration once the response reached new plateau. This was repeated at holding potentials of -25 mV, -50 mV, -75 mV and -100 mV to assess the voltage-dependence of inhibition.

2.12 TEVC *H. axyridis* alkaloid extract (HAE) and harmonine analogue antagonist recordings

For use of HAE, 1 mg was dissolved in 333 μL DMSO solution to make a stock solution of 3 mg/mL. Serial dilutions, from 3 μg/mL to 0.003 μg/mL, were made in the NMDA (10^{-4} M) and glycine (10^{-5} M) agonist solution. The harmonine analogue was dissolved in 10 mL DMSO solution and 300 μL HCl to make a stock solution of 10^{-2} M. Test concentrations were made by diluting stock solution creating 10^{-4} M down to 10^{-7} M concentrations in 10-fold steps. The 4 concentrations made for HAE and the harmonine analogue were tested in the same way as memantine, starting at the lowest concentration, and all tested at the same 4 V_h: -25 mV, -50 mV, -75 mV and -100 mV.

2.13 Data analysis

Measurements of the amplitude were made from the WinEDR recordings before antagonist and at the end of each antagonist interval. This data was then inputted into Microsoft Excel to gather results for inhibition by memantine, HAE and the harmonine analogue. The data points collected from the WinEDR recordings were then transferred across to GraphPad Prism 9 (GraphPad Software, US) and normalised as a percentage of the control response of the NMDAR to the agonist only solution. After normalising, GraphPad Prism 9 was used to generate mean concentration-inhibition graphs. The concentration-inhibition graphs were fitted using the “log(inhibitor) vs. normalized response - Variable slope” non-linear regression equation:

$$\%\ Control\ response = \frac{100}{1+10^{((LogIC_{50}-X)S)}} \quad \textbf{Equation 1}$$

Where X is the logarithm of concentration of the antagonist and S is the Hill slope. This analysis produced IC_{50} values for memantine, HAE and harmonine analogue.

To analyse the decay rate of the NMDAR response on addition of antagonist, the WinEDR recordings were transferred across to WinCP software (Dr John Dempster, Institute of Pharmacy & Biomedical Sciences, University of Strathclyde, UK) and fit with an exponential decay curve to give the time constant in milliseconds.

GraphPad Prism 9 was used for all data analysis, graph plotting and curve fitting as well as application of the Woodhull equation:

$$IC_{50}(V_h) = IC_{50}(0)\, e^{\left(\frac{z\delta VF}{RT}\right)}$$ **Equation 2**

Where δ is the fraction of the membrane electric field sensed by the blocker as it binds, R is the gas constant, T is the absolute temperature, F is Faraday's number and z is the valence of the blocker (= 1 for memantine and 0.5 for HAE and harmonine analogue)

3 Results

3.1 Holding potential effect of NMDA and glycine agonist solution on NMDA receptors

The responses of GluN1-1a/GluN2A NMDARs, expressed in *X. laevis* oocytes, to the agonist solution NMDA (10^{-4} M) and glycine (10^{-5} M) were recorded through TEVC. The oocytes that demonstrated a response were recorded at 4 holding potentials (V_h): -25mV, -50mV, -75mV and -100mV, to investigate the relationship between response sizes and holding potential (Figure 14). The recordings at -75mV and -100mV had larger peak responses recorded compared to the -50mV and -25mV recordings, as seen in Figure 14. The mean current-voltage relationship of NMDAR was investigated by taking the plateau value of the receptor response to NMDA (10^{-4} M) and glycine (10^{-5} M), as shown in Figure 15. The figure highlights that as the V_h becomes more negative, there is a general increase in inward current.

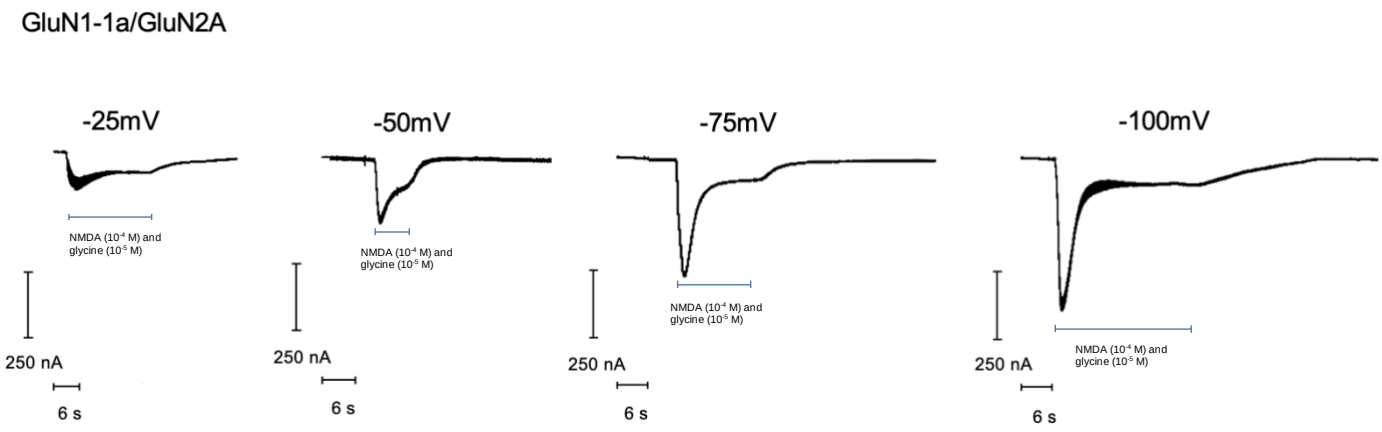

Figure 14. Current recordings of NMDAR, GluN1-1a/GluN2A, responses to NMDA (10^{-4} M) and glycine (10^{-5} M) at -25 mV, -50 mV, -75 mV and -100 mV. The blue bar indicates NMDA (10^{-4} M) and glycine (10^{-5} M) application.

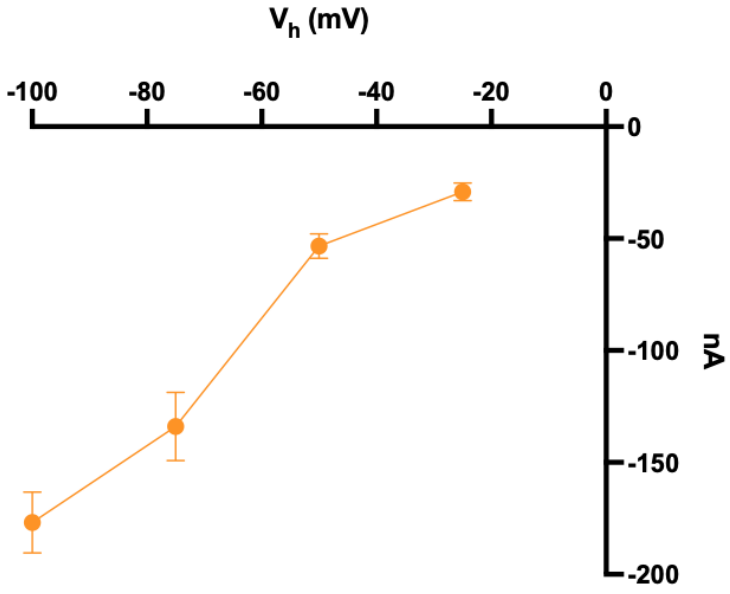

Figure 15. Mean current-voltage relationships (n = 10) for GluN1-1a/GluN2A subunit combination when NMDA (10^{-4} M) and glycine (10^{-5} M) was applied.

3.2 The inhibition of NMDA receptors expressed in *X. laevis* oocytes by memantine

Inhibition of the responses of NMDARs, expressed in *X. laevis* oocytes, to NMDA (10^{-4} M) and glycine (10^{-5} M) by memantine were recorded in a concentration-dependent manner through TEVC at 4 holding potentials: -25 mV, -50 mV, -75 mV and -100 mV. Figure 16 shows an example of what the recordings looked like at -100 mV, showing the staged increase in response inhibition as the concentration of memantine was increased. As the concentrations were increased from 10^{-8} M to 10^{-4} M, increased inhibition was observed until complete inhibition was seen at the point of 10^{-4} M memantine application (Figure 16). The concentration dependent effect of memantine on NMDARs was further highlighted when creating mean concentration-inhibition curves, n=7 (Figure 17).

GluN1-1a/GluN2A

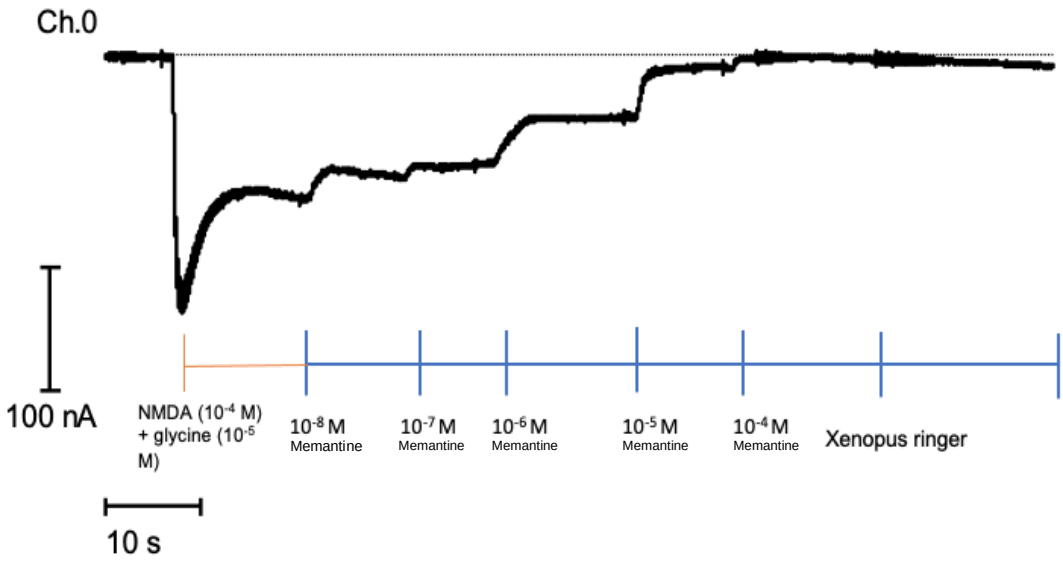

Figure 16. Recording of response at -100 mV, using TEVC, from NMDAR GluN1-1a/GluN2A expressed in *X. laevis* oocytes to NMDA (10^{-4} M) + glycine (10^{-5} M) solution (orange bar) followed by the co-application of memantine. The blue bar indicates the applications of memantine concentrations at intervals after response plateau, starting with 10^{-8} M to 10^{-4} M. Recording finishes with application of MXR. At the point of 10^{-4} M memantine application there was complete inhibition of the receptor response

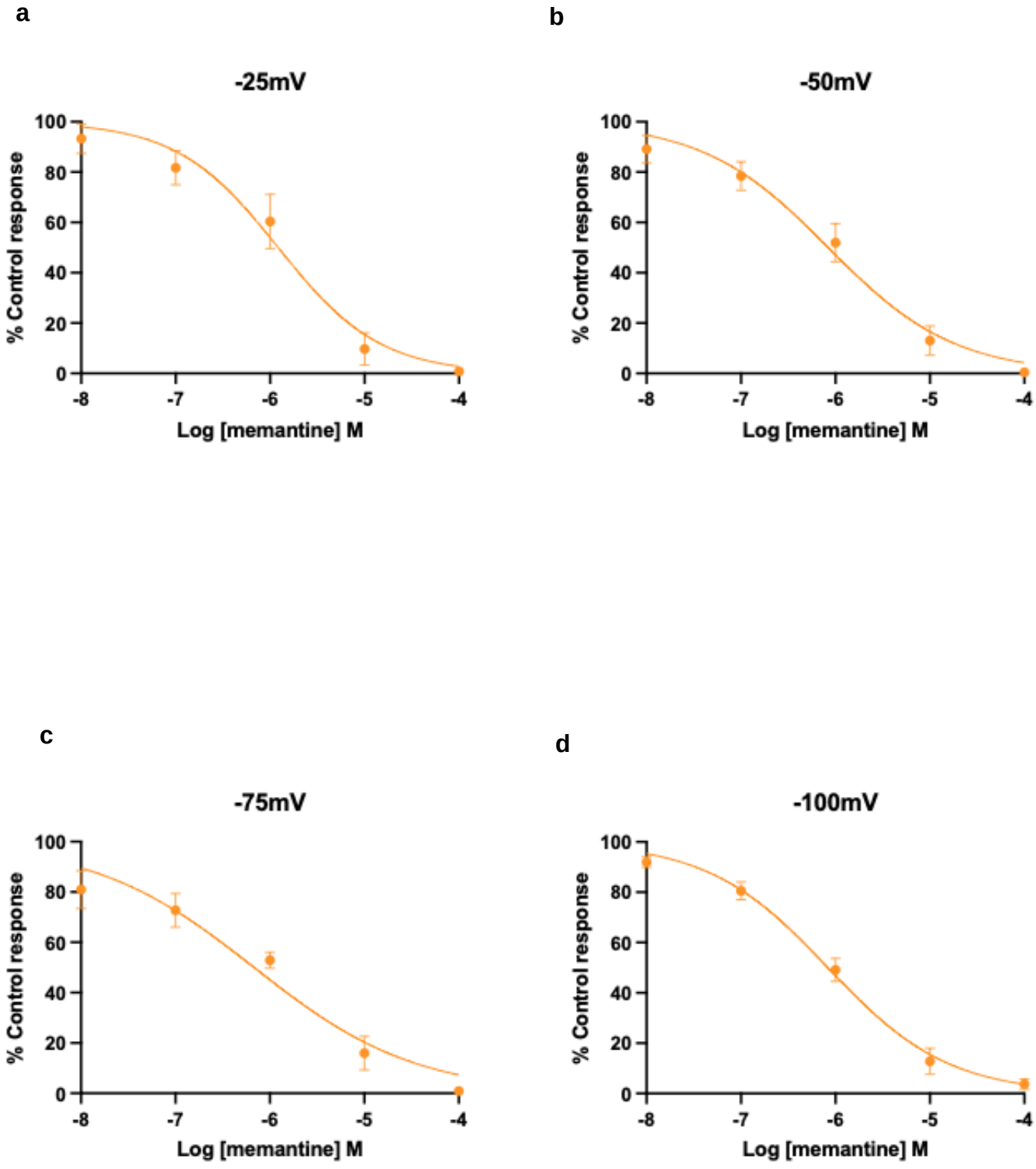

Figure 17. Memantine concentration-inhibition curves demonstrating the concentration-dependent effect of memantine on NMDARs expressed in *X. laevis* oocytes. Recordings taken at -25 mV (a), -50 mV (b), -75 mV (c) and -100 mV (d). Plots represent the Mean ± SEM of 7 replicates per holding potential and are expressed as a percentage of the control response to the agonist solution (NMDA (10^{-4} M) + glycine (10^{-5} M)). Where SEM bar cannot be seen, plot symbol is larger than SEM bar. Curves were generated by Equation 1.

IC_{50} values for the inhibition of GluN1-1a/GluN2A NMDARs by memantine were calculated from the concentration-inhibition curves plotted and fitted and are shown in Table 1. The calculated IC_{50} values showed memantine inhibition is voltage dependent. Memantine had the highest potency on the NMDAR at -75 mV, as shown by the lowest IC_{50} value. The higher IC_{50} values at -25 mV and -50 mV suggests that at a less negative membrane holding potential, memantine has less potency and inhibitory effect. There is also an increase in IC_{50} values from recordings at -75 mV to -100 mV, suggesting memantine becomes slightly less potent a more negative holding potential than -75 mV as well.

Table 1. IC_{50} values and 95% Confidence Intervals (CI) for the inhibition of GluN1-1a/GluN2A NMDARs by memantine at -25 mV, -50 mV, -75 mV and -100 mV. Values estimated from curve fits to data in Figure 17.

	IC_{50} (95% CI) (μM)			
	-25 mV	-50 mV	-75 mV	-100 mV
GluN1-1a/GluN2A	1.22 (0.66-2.16)	0.84 (0.49-1.14)	0.68 (0.35-1.28)	0.83 (0.59-1.16)

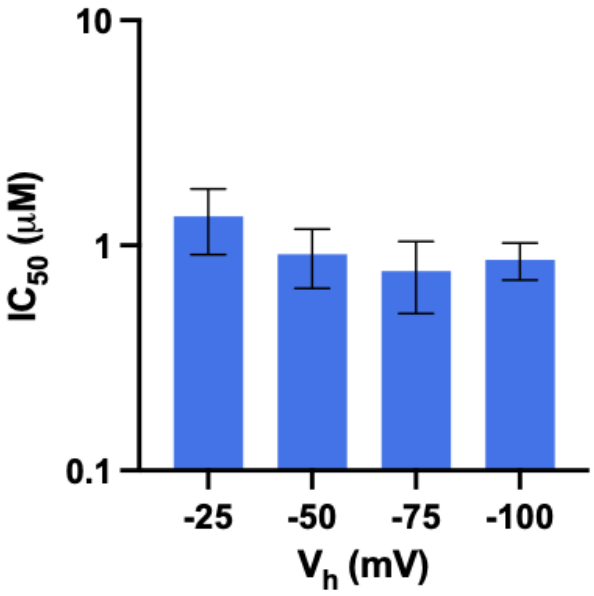

Figure 18. Graph to show the IC_{50} values of memantine with CI's at -25 mV, -50 mV, -75 mV and -100 mV.

The decay rate of the GluN1-1a/GluN2A response when memantine was applied was recorded from the WinEDR recordings by fitting exponential curves to recordings, like that shown in Figure 16, in WinCP. The time constant for onset of inhibition was analysed for concentrations 10^{-6} – 10^{-4} M as these were consistently where the decay rate began to be sizeable. Figure 19 shows that the fastest decay in NMDAR response tended to be around the application of 10^{-6} M memantine (mean decay rate = 837 ms) and the slowest decay rate was during 10^{-5} M memantine application (1530 ms). The mean decay rate time when 10^{-4} M memantine was applied was 953 ms. Looking at the decay rate between the different holding potentials, when the oocyte membrane was set at -25 mV, the decay rate was the most varied during different membrane concentration. Overall, the fastest decay rate times (smallest time constants) were observed when the membrane was set at -75 mV.

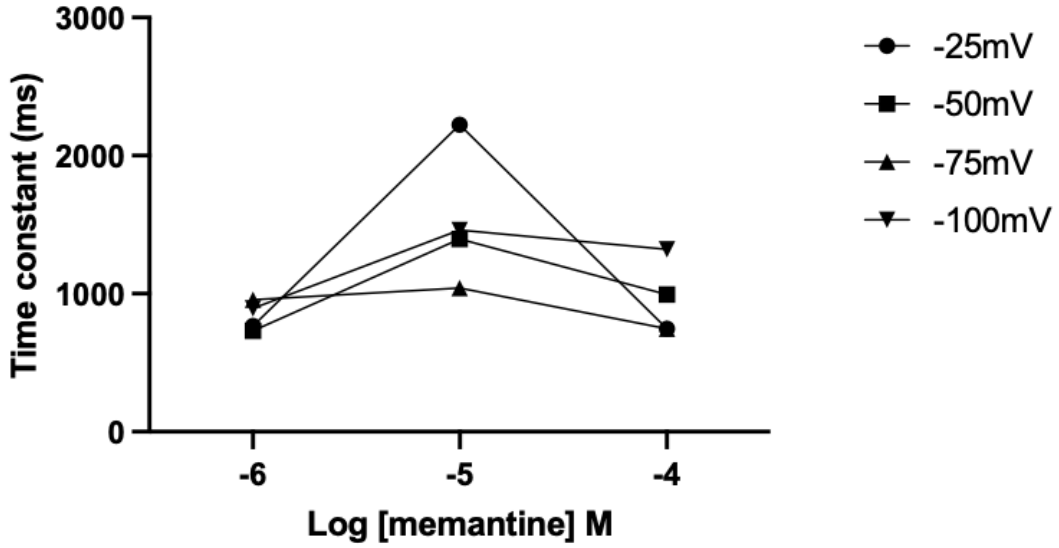

Figure 19. Graph showing the decay time of GluN1-1a/GluN2A response during each phase of memantine concentration application at each of the four holding potentials.

3.3 The inhibition of NMDA receptors expressed in *X. laevis* oocytes by HAE

Inhibition of the responses of NMDARs, expressed in *X. laevis* oocytes, to NMDA (10^{-4} M) and glycine (10^{-5} M) by HAE were recorded in a concentration-dependent manner through TEVC at 4 holding potentials: -25 mV, -50 mV, -75 mV and -100 mV. Figure 20 shows an example of what the recordings looked like at -100 mV, showing the staged increase in response inhibition as the concentration of HAE was increased. As the concentrations were increased from 0.003 μg/mL to 3 μg/mL, increased inhibition was observed (Figure 20). As expected, the higher concentrations of HAE (0.3 μg/mL and 3 μg/mL) demonstrated the most inhibitory effect on the NMDARs response; however, receptors were not completely inhibited at the highest concentration as seen using highest memantine concentrations. The concentration dependent effect of HAE on NMDARs was further highlighted when creating mean concentration-inhibition curves from data collected for n=4 for -25 mV recordings and n=6 for -50 mV, -75 mV and -100 mV (Figure 21).

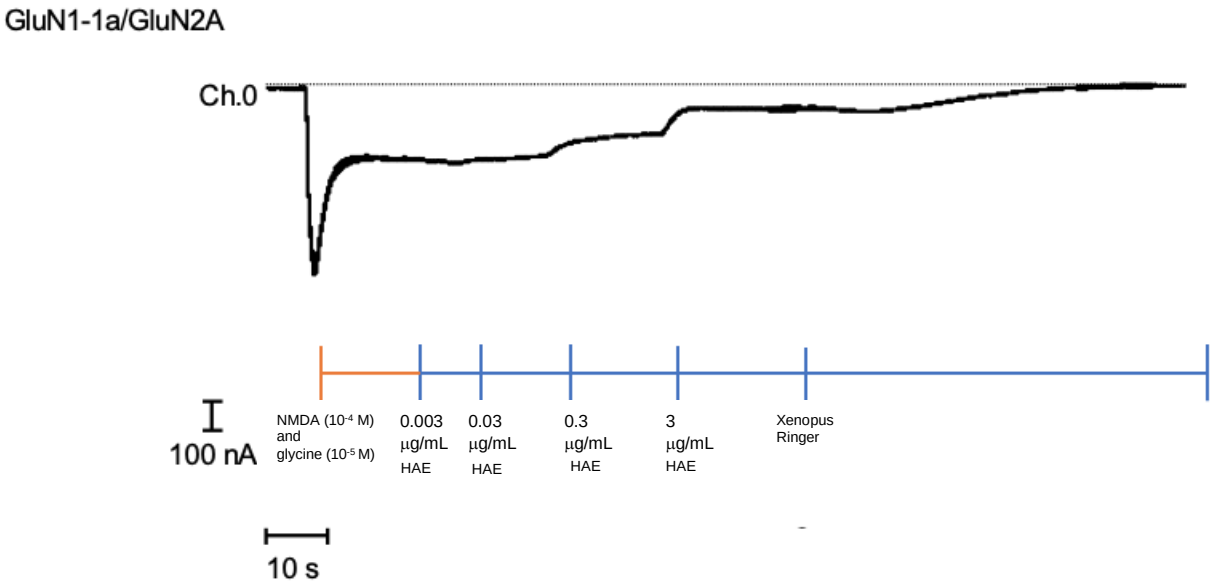

Figure 20. Recording of response at -100 mV, using TEVC, from NMDAR GluN1-1a/GluN2A expressed in *X. laevis* oocytes to NMDA (10^{-4} M) + glycine (10^{-5} M) solution (orange bar) followed by the application of HAE. The blue bar indicates the applications of HAE concentrations at intervals after response plateau, starting with 0.003 μg/mL to 3 μg/mL. Recording finishes with application of MXR.

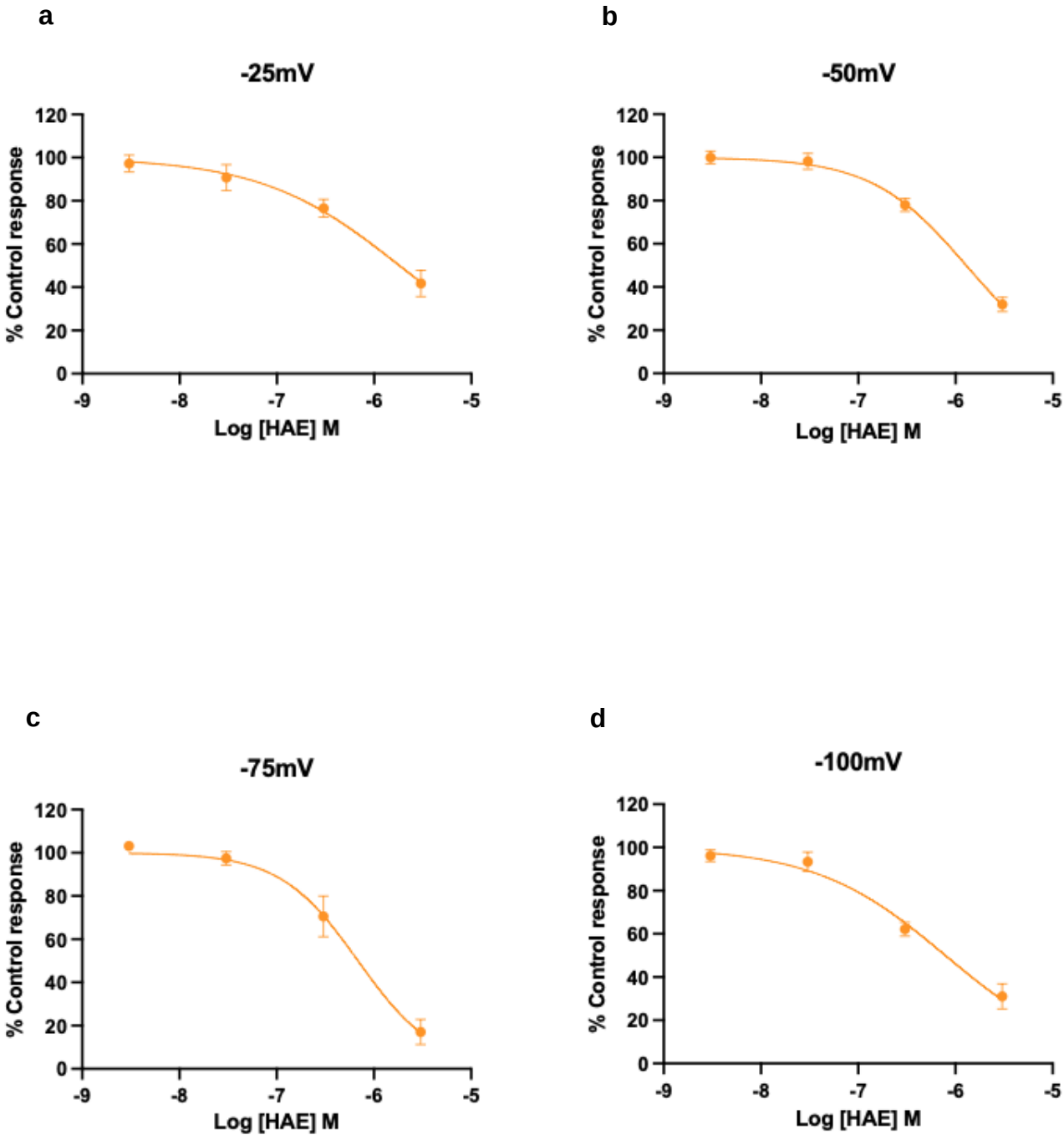

Figure 21. HAE concentration-inhibition curves demonstrating the concentration-dependent effect of HAE on GluN1-1a/GluN2A NMDARs expressed in *X. laevis* oocytes. Recordings taken at -25 mV (a), -50 mV (b), -75 mV (c) and -100 mV (d). Plots represent the Mean ± SEM of 4-6 replicates per holding potential and are expressed as a percentage of the control response to the physiological agonist solution (NMDA (10^{-4} M) + glycine (10^{-5} M)). Where SEM bar cannot be seen, plot symbol is larger than SEM bar. Curves were generated by Equation 1

From the concentration-inhibition curves plotted and fitted, IC_{50} values were calculated, shown in Table 2. The calculated IC_{50} values showed HAE inhibition is voltage dependent. HAE had the highest potency on the NMDAR at -75 mV, as shown by the lowest IC_{50} value. The highest IC_{50} values at -25 mV and -50 mV suggests that at less negative membrane holding potentials, HAE has less potency. There is a significant decrease in IC_{50} value from -25 mV and -50 mV to -75 mV suggesting that HAE becomes significantly more potent across this holding potential range. HAE then becomes less potent as the holding potential gets more negative to -100 mV, shown by the IC_{50} value increasing again.

Table 2. IC_{50} values and 95% CI's for the inhibition of GluN1-1a/GluN2A NMDARs by HAE at -25 mV, -50 mV, -75 mV and -100 mV. Values estimated from curve fits to data in Figure 21. a) IC_{50} values in μg/mL b) IC_{50} values in μM – conversion of HAE values is based upon assumption of HAE being approximately 90% harmonine (282.5 g/mol) and therefore a better comparison to the other compounds can be made

a

	IC_{50} (95% CI) (μg/mL)			
	-25 mV	-50 mV	-75 mV	-100 mV
GluN1-1a/GluN2A	1.82 (1.07-3.69)	1.48 (0.99-1.68)	0.69 (0.45-1.06)	0.79 (0.52-1.23)

b

	IC_{50} (95% CI) (μM)			
	-25 mV	-50 mV	-75 mV	-100 mV
GluN1-1a/GluN2A	6.44 (3.79-13.0)	5.24 (3.50-5.95)	2.44 (1.59-3.75)	2.79 (1.84-4.35)

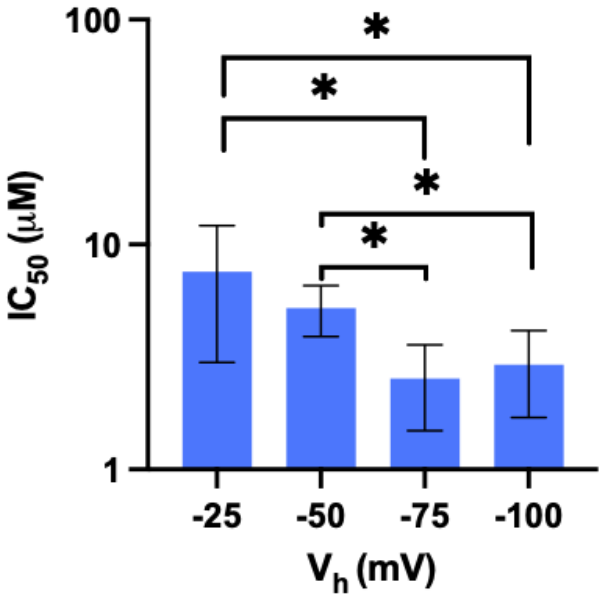

Figure 22. Graph to show the IC_{50} values of memantine with CI's at -25 mV, -50 mV, -75 mV and -100 mV. Significant differences are shown by the *.

The decay rate of the GluN1-1a/GluN2A response when HAE was applied was recorded from the WinEDR recordings by fitting exponential curves to recordings, like that shown in Figure 20, in WinCP. The decay time constant was analysed for concentrations from 0.03 μg/mL to 3 μg/mL as these were consistently where the inhibition was more substantial. Figure 23 shows that the fastest decay in NMDAR response tended to be around the application of 0.3 μg/mL HAE (mean = 743 ms) and the overall slowest decay rate was during 3 μg/mL HAE application (1011 ms). The mean decay rate time when 0.03 μg/mL HAE was applied was 1404 ms. Looking at the decay rate between the different holding potentials there seemed to be a very similar trend other than the significantly slowed onset rate of 3 μg/mL at -75 mV holding potential.

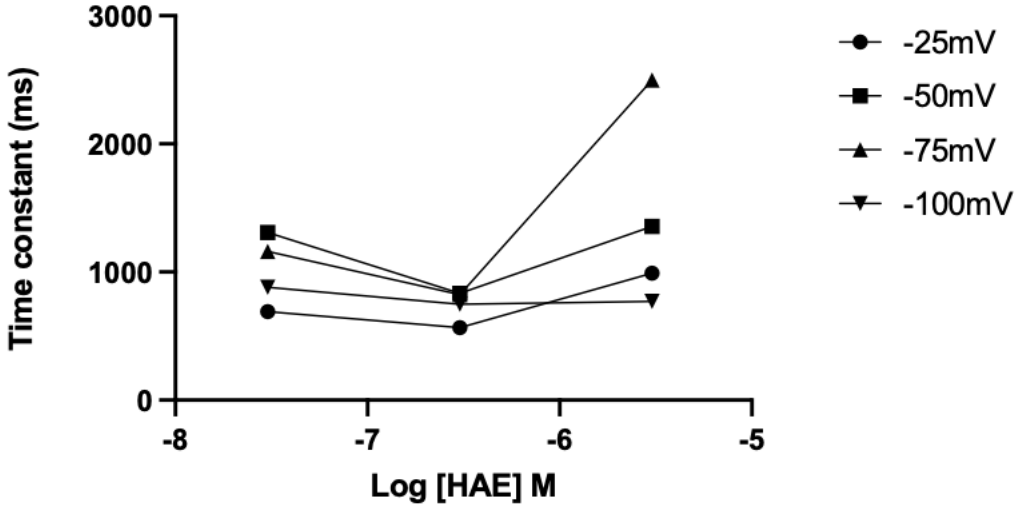

Figure 23. Graph showing the decay time of GluN1-1a/GluN2A response during each phase of HAE concentration application at each of the four holding potentials.

To further explore the binding depth of HAE in comparison to memantine, the effect that the holding potential of the oocyte membrane had on the inhibition of NMDAR responses was analysed. As shown in Figure 24, IC_{50} values for memantine (Table 1) and HAE (Table 2b) were plotted against V_h and then fitted with the Woodhull equation (Equation 2) (Woodhull, 1973). The mixed composition of HAE meant that an accurate *z* value could not be assigned, so *z* and δ were combined for both HAE and memantine equation fitting. The zδ values were 0.1727 for memantine and 0.3510 for HAE but due to HAE having two positive charges on the main compound harmonine, the zδ value is divided by 2. Therefore, the δ values are very similar, 0.1727 and 0.1755, implying that the binding depth within the NMDAR channel was similar for both compounds. The slope of the Woodhull-fitted regression for memantine differed significantly from zero ($P = 0.0089$) and same for HAE ($P = 0.0079$). Thus, indicating strong voltage-dependency of inhibition by memantine and HAE.

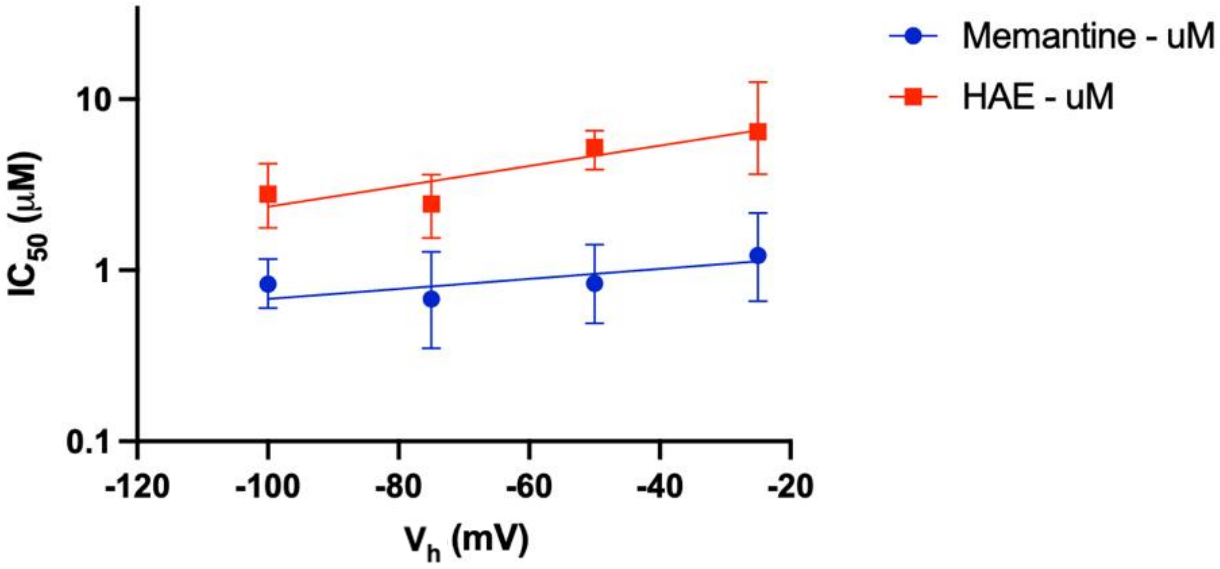

Figure 24. IC_{50} values were plotted for memantine and HAE against V_h and fitted with the Woodhull equation (Equation 2). The slope of the curves (0.1727 memantine and 0.1755 HAE) is significantly greater than 0 ($P = 0.0089$ and $P = 0.0079$) indicating voltage-dependent inhibition of NMDAR by memantine and HAE. A similar slope also suggests similar binding depth within receptor pore.

3.4 The inhibition of NMDA receptors expressed in *X. laevis* oocytes by harmonine analogue

Inhibition of the responses of GluN1-1a/GluN2A NMDARs, expressed in *X. laevis* oocytes, to NMDA (10^{-4} M) and glycine (10^{-5} M) by the harmonine analogue was recorded through TEVC at 4 holding potentials: -25 mV, -50 mV, -75 mV and -100 mV. Figure 25 shows an example of what the recordings looked like at -100 mV, showing the staged increase in response inhibition as the concentration of the harmonine analogue was increased. As the concentrations were increased from 10^{-7} M to 10^{-4} M, increased inhibition was observed (Figure 25). The highest concentration of the analogue used, 10^{-4} M, demonstrated complete inhibition of the NMDAR response nearly every time: similar to the application of memantine. The concentration dependent effect of the analogue on NMDARs was further highlighted when creating mean concentration-inhibition curves from data collected for n=2 for -25 mV recordings and n=4 for -50 mV, -75 mV and -100 mV (Figure 26).

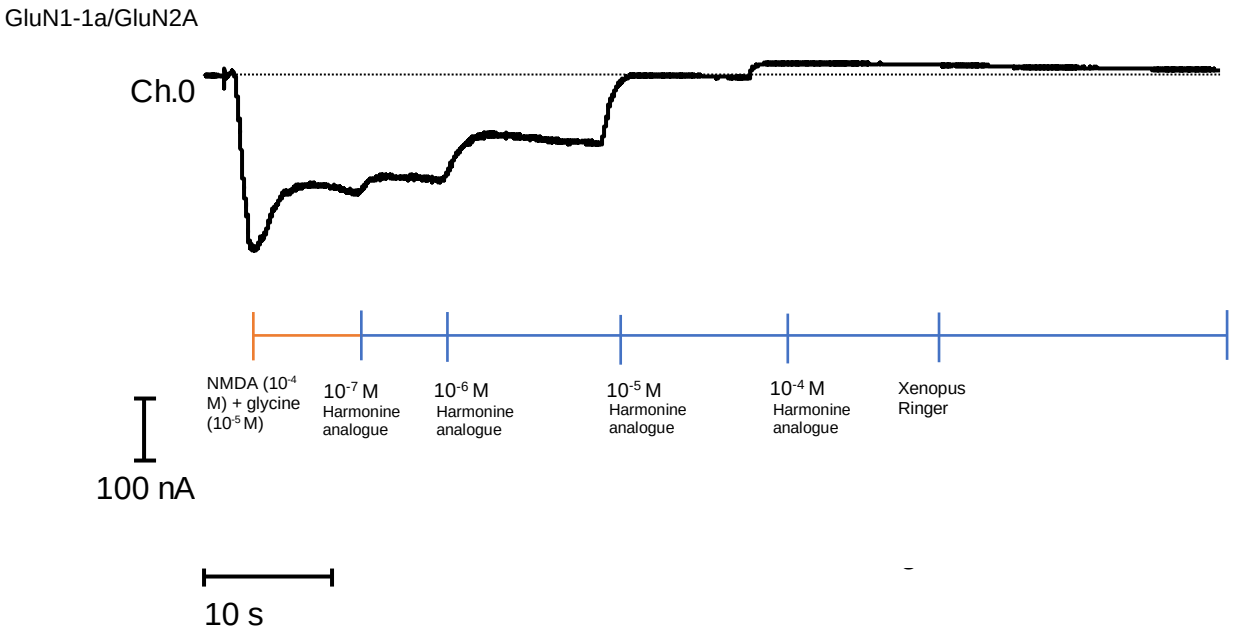

Figure 25. Recording of response at -100 mV, using TEVC, from NMDAR GluN1-1a/GluN2A expressed in *X. laevis* oocytes to NMDA (10^{-4} M) + glycine (10^{-5} M) solution (orange bar) followed by the application of the harmonine analogue. The blue bar indicates the applications of analogue concentrations at intervals after response plateau, starting with 10^{-7} M and progressing to 10^{-4} M. Recording finishes with application of MXR.

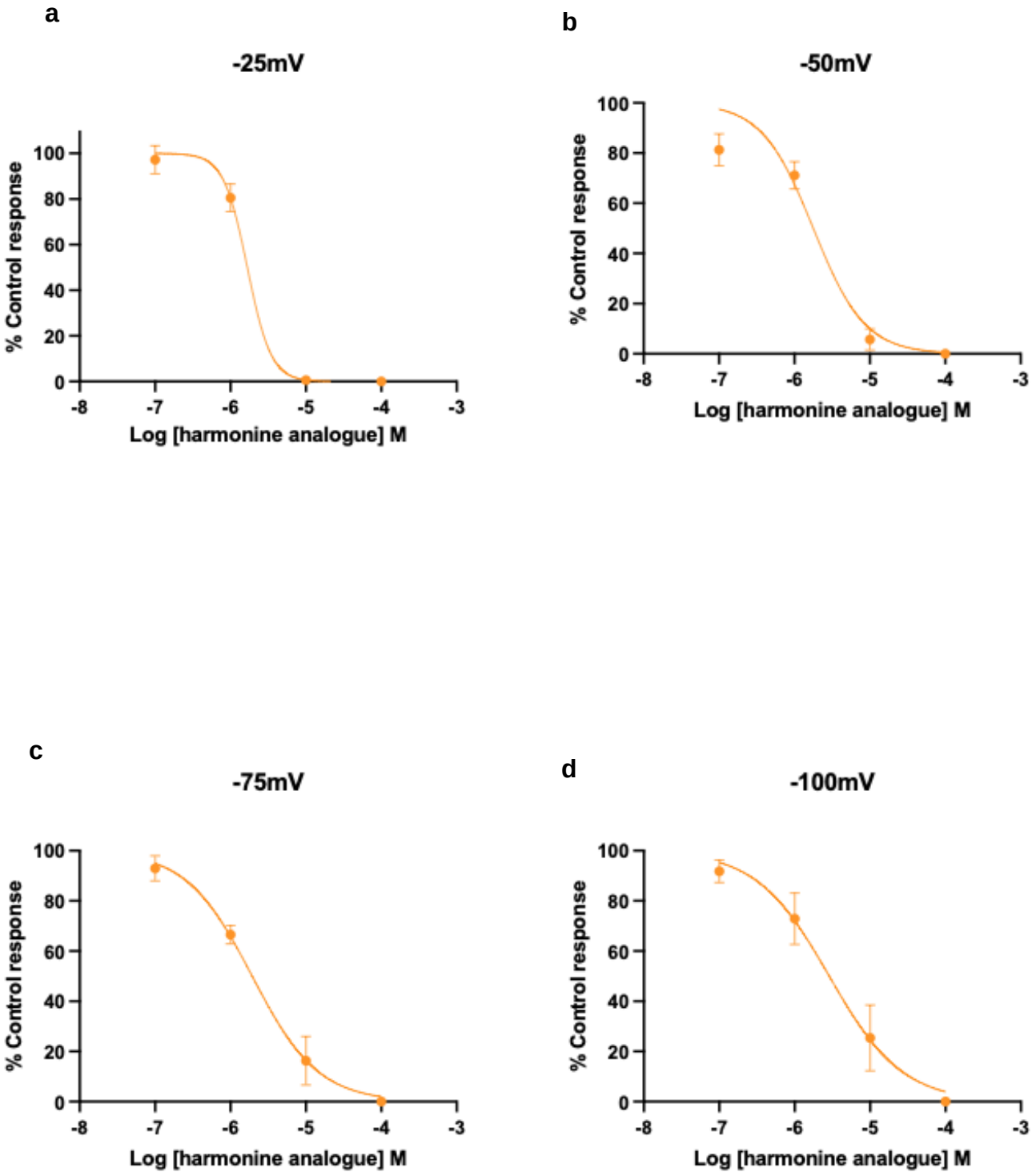

Figure 26. Harmonine analogue concentration-inhibition curves demonstrating the concentration-dependent effect of the analogue on NMDARs expressed in *X. laevis* oocytes. Recordings taken at -25 mV (a), -50 mV (b), -75 mV (c) and -100 mV (d). Plots represent the Mean ± SEM of 2-4 replicates per holding potential and are expressed as a percentage of the control response to the agonist solution (NMDA (10^{-4} M) + glycine (10^{-5} M)). Where SEM bar cannot be seen, plot symbol is larger than SEM bar. Curves were generated by Equation 1.

IC_{50} values for the inhibition of GluN1-1a/GluN2A NMDAR by the harmonine analogue were calculated from the concentration-inhibition curves plotted and fitted, shown in Table 3. The calculated IC_{50} values showed the harmonine analogue inhibition is voltage. The analogue had the highest potency and inhibitory effect on the NMDAR at -25 mV as shown by the lowest IC_{50} value in Table 3. The higher IC_{50} values at -75 mV and -100 mV, and the large increase in IC_{50} value between these membrane holding potentials, suggests that a more negative membrane holding potential the analogue has less potency and inhibitory effect.

Table 3. IC_{50} values and 95% CIs for the inhibition of GluN1-1a/GluN2A NMDARs by harmonine analogue at -25 mV, -50 mV, -75 mV and -100 mV (n = 2-4). Values estimated from curve fits to data in Figure 26. Where CIs are not listed, the sample size was too small (at -25mV n=2).

	IC_{50} (95%) (μM)			
	-25 mV	-50 mV	-75 mV	-100 mV
GluN1-1a/GluN2A	1.67	1.78 (1.09-2.82)	1.94 (1.26-3.02)	2.88 (1.42-5.74)

Looking more specifically at results taken at 4 holding potentials across one individual cell, IC_{50} values from this cell were calculated using Equation 1 and are as shown in Table 4. The IC_{50} values support that the harmonine analogue acts in a voltage dependent way for potency and inhibition but when analysing results from only one cell, the IC_{50} value trend across the V_h is significantly more in line with the data from memantine and HAE. Here it can be seen that then highest IC_{50} values are from V_h of -25 mV and -50 mV and then the analogue becomes more potent at lower V_h, specifically at -75 mV as expected.

Table 4. IC_{50} values for the inhibition of GluN1-1a/GluN2A NMDARs by harmonine analogue at -25 mV, -50 mV, -75 mV and -100 mV (n = 1). Values estimated from Equation 1. Confidence Intervals not calculated due to sample size n=1.

	IC_{50} (μM)			
	-25 mV	-50 mV	-75 mV	-100 mV
GluN1-1a/GluN2A	1.65	1.55	1.08	1.49

The decay rate of the GluN1-1a/GluN2A response when the harmonine analogue was applied was recorded from the WinEDR recordings by fitting exponential curves to recordings, like that shown in Figure 25, in WinCP. The time constant for onset of inhibition was analysed for concentrations 10^{-6} – 10^{-4} M as these were consistently where the decay rate began to be substantial. Figure 27 shows that the fastest decay in NMDAR response tended to be around the application of concentration 10^{-4} M (mean = 382 ms) and the slowest mean decay rate was during 10^{-6} M memantine application (1107 ms). The mean decay rate time when 10^{-5} M of the harmonine analogue was applied was 786 ms. Looking at the decay rate between the different holding potentials, the fastest decay rate time (the smallest time constant) was observed when the membrane was set at -75 mV. Looking at the decay rate between the different holding potentials there seemed to be a very similar trend other than the significantly slowed onset rate of 10^{-5} M harmonine analogue at -50 mV.

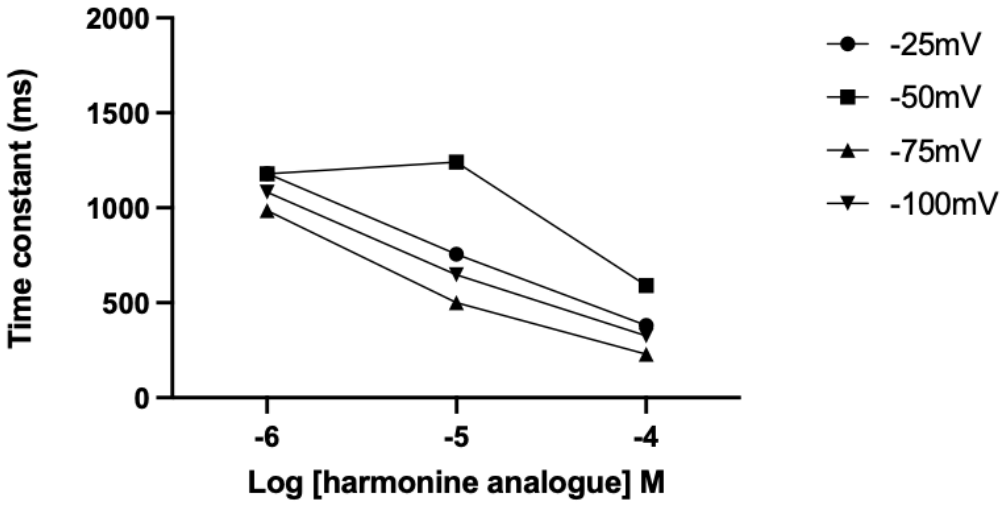

Figure 27. Graph showing the decay time of GluN1-1a/GluN2A response during each phase of the harmonine analogue concentration's application at each of the four holding potentials.

To further support the voltage dependency of harmonine analogues action on NMDAR, the IC_{50} values from Table 4 were plotted against V_h and fitted with the Woodhull regression equation (Equation 2) (Figure 28) (Woodhull, 1973). The slope of the Woodhull-fitted regression differed significantly from zero (P = 0.0085) and this confirms the voltage dependency of the harmonine analogue. From the Woodhull

regression equation, the zδ value was 0.0701 and because the z value is 2, the δ value was 0.035. The δ value for the harmonine analogue was less than those collected for memantine and HAE suggesting the binding depth of the analogue was shallower towards the extracellular side within the NMDAR channel.

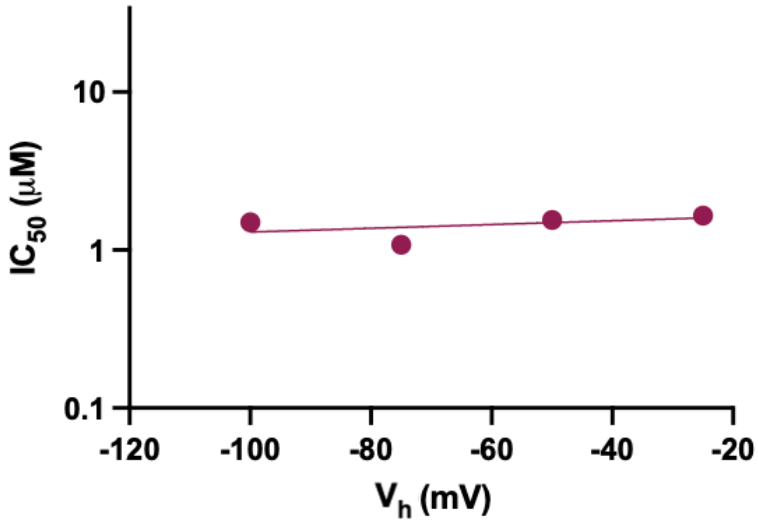

Figure 28. IC_{50} values were plotted for harmonine analogue n=1 (Table 4) against V_h and fitted with the Woodhull equation (Equation 2). The slope of the curves (0.07) is significantly greater than 0 ($P = 0.0085$) indicating voltage-dependent inhibition of NMDAR by harmonine analogue.

4 Discussion

4.1 The inhibition of NMDA receptors expressed in *X. laevis* oocytes by memantine

Memantine was shown to have the most potent inhibition of NMDAR responses when the oocyte was set at a holding potential of -75 mV (IC_{50} = 0.68 μM). The results for the more negative potential at -100 mV (IC_{50} = 0.83 μM) showed memantine to be less potent at this holding potential in comparison to -75 mV. The IC_{50} values showed also that memantine was significantly less potent at -25 mV (IC_{50} = 1.22 μM) and at -50 mV holding potential, IC_{50} value 0.84 μM, memantine had similar potency to holding potential of -100 mV. These IC_{50} values confirmed that overall memantine is highly potent at the GluN1-1a/GluN2A NMDAR subtype which has been observed in other papers where memantine inhibited the same subunit combination at IC_{50} values of 1.25 μM, 0.9 μM, 1.33 μM and 0.79 μM at holding

potentials around -70 mV (Kotermanski et al., 2009; Chen and Lipton, 2005; Glasgow et al., 2017; Gilling et al., 2009). Memantine's tolerability is thought to be due to the approximate 1 μM $IC_{50,}$ giving a good point of reference for comparison of the harmonine based compounds later. Even though some of these studies used different electrophysiology techniques for data collection, for example whole cell patch clamp techniques, the concentrations of memantine and the holding potentials were similar and therefore confirmed that memantine acts in a concentration and voltage dependent manner as expected.

There is thought that the slight increase in IC_{50} value recorded from -75 mV (0.68 μM) to -100 mV (0.83 μM) may be explained through the idea that memantine is an open channel blocker. It is thought that across a certain range of holding potentials, as you decrease the holding potential and make it more negative, memantine becomes more potent and therefore the IC_{50} value becomes smaller. This was observed across the results as the IC_{50} values started at 1.22 μM at -25 mV, then to 0.84 μM at -50 mV and decreased to the lowest value of 0.68 μM at -75 mV. This trend could be described by the fact that memantine is more able to inhibit ion permeation under weak depolarisation (around -50 mV to -75 mV) which is often caused by the pathological leakage of glutamate into the synapse or remaining glutamate from pathologically reduced uptake (Figure 6) (Parsons et al., 2013). This leakage means that there is prolonged activation of the receptors in which the memantine can become an effective blocker, even more so at -75 mV than -50 mV membrane holding potential. It is also known that memantine has reduced inhibition ability at more depolarised potentials like -25mV as it dissociates, which permits the physiological activity, and this is consistent with the higher IC_{50} value at -25mV. However, the slight increase in the IC_{50} value at -75 mV up to the value at -100 mV may be explained by memantine binding reaching maximum inhibition and during this, due to the low negative potential, there is a strong driving force that acts strongly on the memantine to push it all the way through the pore and out the other side. This therefore causes a reduction of blocking, reducing some of the inhibitory effects seen at more positive holding potentials like -75 mV and -50 mV. Less inhibition results in more permeation and leakage through the pore and would therefore contribute to the larger IC_{50} values observed.

4.2 The inhibition of NMDA receptors expressed in *X. laevis* oocytes by HAE

The highest concentration of HAE applied (3 μg/mL) resulted in significant inhibition, sometimes complete, of the GluN1-1a/GluN2A subunit NMDAR response (Figure 19). This was expected to be observed as previous work showed inhibitory effects of HAE on rat GluN1-1a/2A receptor subtypes, at similar concentrations. The other concentrations used of HAE, 0.3 - 0.003 μg/mL, resulted in very little inhibitory effect on the receptor response, with virtually no change in response when 0.03-0.003 μg/mL was applied. At the highest concentration of HAE used, 3 μg/mL, the level of inhibition depended on the holding potential that was set. At the more negative holding potentials, greater levels of receptor inhibition were observed (Figure 20). Thus, supporting that HAE acts in a voltage and concentration dependent manner like memantine.

HAE was shown to have the least potency of inhibition when the holding potential of the oocyte was at -25 mV (IC_{50} = 1.82 μg/mL) and this suggests that HAE has least potency and inhibitory action at the more positive membrane potentials. This was confirmed by the lower IC_{50} at -50 mV (1.48 μg/mL). Decreasing the holding potential of the membrane from -50 mV to -75 mV meant the IC_{50} here significantly dropped (IC_{50} = 0.69 μg/mL). At this holding potential HAE was seen to have the most potent inhibitory effect as when the holding potential was decreased further, down to -100 mV, the IC_{50} increased slightly up to 0.79 μg/mL. Interestingly, this trend in potency increasing as the holding potential of the membrane decreases until the decrease at -100 mV, followed the same trend as observed for the memantine IC_{50} values across the same 4 holding potentials. The same explanation discussed for memantine may therefore be applied to explain the increase in potency from -25 mV to -75 mV; the HAE becomes a stronger response inhibitor during ‘background noise’ activation of NMDARs. The increase in IC_{50} from -75 mV to -100 mV may also be explained in the same way as memantine; the HAE block may be pushed all the way through the NMDAR channel at -100mV due to the strong driving force so the inhibition levels by HAE decrease due to the molecule no longer being present in the pore. It may also be assumed that HAE works in the same way as an open channel blocker due to this trend in potency and action.

Assuming the main component of HAE tested is harmonine as discussed, this research highlights that harmonine acts in a similar way to memantine and therefore supports its potential use as a therapeutic for AD. As discussed previously, studies have also shown that HAE has inhibitory effects on AChE which is another therapeutic target (Patel, 2017). Therefore, harmonine, is thought to have multitarget properties; further strengthening its therapeutic potential due to the role of AChE and NMDARs in AD pathology. However, to understand the full potential of harmonine in AD treatment, it would be appropriate to investigate higher concentrations than used in this study (3 μg/mL). Higher concentrations should be more effective to reach full inhibition of the receptor response at all holding potentials investigated, as observed when using memantine.

4.3 Comparison of memantine and HAE inhibition

As discussed, HAE did show potent inhibition at the NMDARs, but the maximum inhibition seen was not as great as memantine. This is likely due to the highest concentration of HAE being around 10-fold lower than the highest concentration used of memantine. To draw more accurate comparisons between the inhibitory effects of memantine and HAE, the concentration units of HAE were converted from μg/mL to μM (see conversions of units between Table 2a and Table 2b). The different unit that the values of HAE were measured in was due to the likely presence of several other alkaloid compounds that are present in HAE. This conversion was based upon the assumption that HAE is approximately 90% harmonine and the molecular weight of harmonine being 282.5 g/mol. This therefore meant that the highest concentration used of HAE equates to 10.62 μM and the highest concentration used of memantine was 100 μM; about 10 times smaller as aforementioned.

Drawing direct comparisons of the IC_{50} values calculated at -75 mV for both memantine and harmonine gives an insight as to whether harmonine would potentially work at clinically acceptable levels. However, once the IC_{50} value is converted for HAE, it is 2.44 μM in comparison to the value found for memantine which was 0.68 μM. As previously discussed, the clinically acceptable level of IC_{50} value is around 0.7-1.7 μM and this therefore suggests that harmonine may not be

clinically tolerated. The higher dose of harmonine that would be required to see sufficient inhibitory effects may induce an unacceptable level of adverse effects, including increased inhibition of nAChRs and other targets that are presently unknown. When looking at the NMDAR response decay rate by HAE (Figure 23) and comparing it to the decay rates when memantine was applied (Figure 19), the overall time constants for each concentration ranged from 743 to 1530 ms. The decay rates of the response when using HAE are similar to that observed by memantine as the range of time constants were within a similar range.

Further analysis was carried out on the NMDAR to explore the mode of action of HAE inhibition in comparison to memantine. Inhibition was shown to be voltage dependent for both compounds as previously discussed but this was further confirmed by analysis of the voltage dependency by using the Woodhull equation (Figure 24) (Woodhull, 1973). The slope of the Woodhull-fitted regression for memantine differed significantly from zero (P = 0.0089) and same for HAE (P = 0.0079). Thus, indicating strong voltage-dependency of inhibition by memantine and HAE. The results from this analysis (Figure 24) showed HAE to act in a similar way to memantine and highlighted that its actions were consistent with the actions of an open channel blocker. The $z\delta$ values being so similar, between memantine (0.1727) and HAE (0.1755), suggests also that their binding sites are in similar regions and depth within the NMDAR pore. Therefore, suggesting that HAE may bind at the Mg^{2+} ion binding site of the NMDARs like memantine.

4.4 The inhibition of NMDA receptors expressed in *X. laevis* oocytes by a harmonine analogue

To continue the investigation of harmonine NMDAR inhibition, a synthetic harmonine analogue was used to investigate the inhibitory effects on NMDARs. The analogue was shown to inhibit the receptor responses in a concentration and voltage dependent manner as well. The voltage dependency was confirmed by fitting the IC_{50} values to the Woodhull regression equation (Figure 28). The slope differed significantly from zero (P = 0.0085) and therefore confirms the voltage dependency of the harmonine analogue. The highest concentration (10^{-4} M) of analogue used resulted in complete inhibition of the receptor response; this also regularly occurred

when 10^{-5} M concentration was applied (Figure 25). The lower concentrations, 10^{-6} M and 10^{-7} M resulted in less response inhibition, but significant inhibition was still observed. Thus, confirming the concentration dependent action, as was expected. The inhibitory action of the harmonine analogue also confirmed that the action of HAE inhibition observed in the other section of the research was due to the large harmonine component as discussed.

The harmonine analogue appeared to have most potent inhibition at -25mV when observed using a low and variable sample size (because of oocyte quality) of n=2-4 (Table 3), but this was likely masking any consistent relationship between inhibition and V_h. However, when analysing one individual cell where data was collected across all holding potentials (Table 4), a relationship just like those for memantine and HAE was seen, whereby, inhibition was greatest at -75 mV, dropping off either side of that.

The higher IC_{50} values at the more positive membrane potentials (-25 mV and -50 mV) may be explained by the theory applied to memantine inhibition at these holding potentials. If the analogue acts in a similar way to memantine, then it is likely that it dissociates during physiological activation. However, when the channels are activated by glutamate leakage or decreased glutamate uptake in the synapse, causing weak depolarisation levels (-50 mV to -75mV), the analogue can work as a highly effective channel blocker (Parsons et al., 2013). The increase in IC_{50} between -75 mV and -100 mV may again be explained by the analogue reaching maximum inhibition at the receptor and the more extreme negative potential of -100 mV causing a strong driving force that pushes the analogue all the way through the receptor channel so that there is no longer block in the pore and therefore less inhibition occurs. Overall, the findings from investigating the inhibition by the harmonine analogue showed the compound to be an active inhibitor and therefore opens the possibility of its use to be further investigated as a potential therapeutic treatment for AD.

4.5 Comparison of inhibition of harmonine analogue with the inhibition of memantine and HAE

Due to the harmonine analogue being a pure compound, the units of concentration were μM and therefore the converted values of HAE were used for comparison to the analogue (see Table 2b). As discussed, the harmonine analogue acted in similar voltage and concentration dependent ways to the other two antagonists tested and therefore it has the potential to be considered an effective NMDAR open channel blocker. When looking at the decay rates of the NMDAR responses when applying memantine, HAE and the harmonine analogue, the time constant ranges between 383 ms (harmonine analogue at 10^{-4} M) and 1530 (memantine at 10^{-6} M). Overall, the response decay rates are quite similar, and this is important for new compounds to act in a similar way to memantine. Interestingly, the concentrations needed of the analogue to achieve the 50% inhibition of the NMDAR response, shown by the IC_{50} values, were more in line with that of memantine as opposed to HAE. When looking at the IC_{50} value generated for the analogue at -75 mV, 1.08 μM, it is similar to that found for memantine in this study (0.68 μM) and also similar to the IC_{50} values found for memantine in other papers (Kotermanski et al., 2009; Chen and Lipton, 2005; Glasgow et al., 2017; Gilling et al., 2009). Therefore, the harmonine analogue has the potential to be clinically tolerated due to the lower concentrations required for sufficient inhibition and this supports its potential use as a therapeutic treatment for AD.

4.6 Selectivity of memantine and HAE between human and rat NMDARs

Previous work completed to investigate the inhibitory effects of memantine on rat GluN1-1a/GluN2A NMDARs meant that the IC_{50} values from Table 1, memantine inhibiting human NMDARs, could be compared. Kaur (2021) found the IC_{50} values of memantine inhibition of rat GluN1-1a/GluN2A NMDARs as follows; -50 mV = 4.19 μM**,** -75 mV = 1.45 μM and -100 mV = 1.84 μM. Drawing comparisons between these IC_{50} values and the values collected in this study for inhibition of human GluN1-1a/GluN2A NMDARs by memantine (Table 1), it can be seen that the selectivity and potency of memantine appeared to be higher towards the human NMDARs (shown by the lower IC_{50} values). The trend across the IC_{50}s was similar between human and rat response inhibition, with a lower potency at V_h -50 mV and -

100 mV and the highest potency at -75 mV. Memantine was regularly tested on rat NMDARs during previous clinical trials, therefore collecting data to observe its inhibitory action on human NMDARs gives a better insight into how it may work during human therapeutic treatment for AD. Human NMDAR clone data also provides better data for comparisons of other compounds when their actions are assessed on human receptors.

Previous work done on the inhibitory effects of HAE on rat GluN1-1a/GluN2A NMDARs meant that the IC_{50} values from Table 2, HAE inhibiting human NMDARs, could be compared. Kaur (2021) found the IC_{50} values of HAE inhibition on rat GluN1-1a/GluN2A NMDARs as follows; -50 mV = 2.65 µg/mL**,** -75 mV = 1.11 µg/mL and -100 mV = 1.72 µg/mL. Drawing comparisons between these IC_{50} values and the values collected in this study for inhibition of human GluN1-1a/GluN2A NMDARs by HAE (Table 2), it shows that the selectivity and potency of HAE is higher towards the human NMDARs (shown by the significantly lower IC_{50} values for the human clones). The trend across the IC_{50}'s was similar between human and rat response inhibition, with a lower potency at V_h -50 mV and -100 mV and the highest potency at -75 mV. Up until now, research into HAE was carried out primarily on rat NMDARs, making this data for human NMDAR inhibition novel (Kaur, 2021; Patel, 2017; Chen and Lipton, 2005). It is essential to investigate the effects of an antagonist on human clones as well as rat before it can be really considered as a therapeutic treatment, however the sample size across this research is relatively small and therefore this research needs to be continued. Importantly, memantine and HAE were both more potent, shown by the IC_{50} values, on the human NMDARs. The lower clinically useful level of the compounds is likely to reduce adverse effects or abuse potential.

4.7 Future work

To further support the potential of harmonine and harmonine analogues as therapeutic treatments for AD, more research needs to be carried out to see the dissociation rates of these compounds on NMDARs. It would be important to analyse the dissociation rates of memantine on the human NMDAR clones using GluN1-1a/GluN2A and other subunit combinations for reference. Then from this, the dissociation rates of HAE and the analogue should be assessed to ensure that they

dissociate from the NMDAR in a similar way to memantine. This would hopefully show that they have the potential to not detrimentally build to the receptor, allowing for normal function of the NMDARs and therefore reducing adverse effects or abuse potential. Looking more specifically at future work involving HAE, higher concentrations (> 3 μg/mL) of HAE could be used to investigate the potential of HAE to completely inhibit the NMDAR response like memantine, as opposed to the partial inhibition seen in the data.

To really understand the therapeutic potential of the harmonine analogue used, a greater sample size would be required as during this research the maximum sample size was n=4 (at -50 mV, -75 mV and -100 mV) and n=2 when holding potential was set to -25 mV. As can be seen from Table 3 and 4, the data collected from multiple different cells showed a very different trend across the holding potentials and I would therefore suggest using a larger sample size where data is collected for each holding potential, at each concentration, in each oocyte cell. This avoids the barriers faced in this part of the research where the quality of the cell impacted the longevity of experiments and the ability to record at the more extreme membrane potentials. I would also suggest this for future work on any electrophysiology analysis, including HAE, as this work highlighted this as an issue. The sample size of the inhibitory effects of HAE and the analogue should also stretch to other subunit combinations as thus far, they have only been tested on the human GluN1-1a/GluN2A subunit combination. As aforementioned, the GluN2 component of the receptor often decides the pharmacological properties of the receptor so investigating the inhibitory effect of these compounds on the different GluN2 subunits is necessary. Investigating the action of HAE and the analogue specifically on GluN2B receptors would be important as these receptors are often found extrasynaptically and therefore may be more susceptible to glutamate leakage and reduced uptake (Liu et al., 2019). It would also be very beneficial to investigate the inhibitory effects of the harmonine analogue on AChE to see if the analogue has the same potential as a multitarget to target both the glutamatergic system and cholinergic system. Due to the potential that this analogue shows, it would also be greatly beneficial to investigate the effects of other analogues of harmonine.

5 Conclusion

Using TEVC electrophysiology, this study found that memantine, HAE and the harmonine analogue did act in a voltage and concentration dependent manner for the inhibition of the human GluN1-1a/GluN2A subunit combination of NMDARs. HAE and the analogue appeared to act in a very similar way to the clinically tolerated drug treatment memantine. The harmonine analogue acted in a more similar way than HAE, as the concentrations required to reach complete response inhibition at all holding potentials was lower. Therefore, further work into this harmonine analogue and other harmonine analogues, to see their action in larger sample sizes and on other NMDAR subtypes, would give a great insight into their true potential as treatments. HAE has been previously reported to act in the way of memantine to inhibit nAChRs, and harmonine has been shown to inhibit AChE, therefore, this should be also investigated for the harmonine analogue. Strong inhibitory action and multitarget ligand is a good route for a therapeutic treatment and therefore this research has created a case to suggest that HAE and harmonine analogues are a good route to investigate for the future of AD treatment.

6 References

Adlimoghaddam, A., Neuendorff, M., Roy, B. & Albensi, B. C. 2018. A review of clinical treatment considerations of donepezil in severe Alzheimer's disease. *CNS neuroscience & therapeutics,* 24**,** 876-888.

Alam, N., Choi, I.-S., Song, K.-S., Hong, J.-K., Lee, C. O. & Jung, J. H. 2002. A new alkaloid from two coccinellid beetles Harmonia axyridis and Aiolocaria hexaspilota. *Bulletin of the Korean Chemical Society,* 23**,** 497-499.

Alberdi, E., Sánchez-Gómez, M. V., Cavaliere, F., Pérez-Samartín, A., Zugaza, J. L., Trullas, R., Domercq, M. & Matute, C. 2010. Amyloid β oligomers induce Ca2+ dysregulation and neuronal death through activation of ionotropic glutamate receptors. *Cell calcium,* 47**,** 264-272.

Anand, R., Gill, K. D. & Mahdi, A. A. 2014. Therapeutics of Alzheimer's disease: Past, present and future. *Neuropharmacology,* 76**,** 27-50.

Aracava, Y., Pereira, E. F., Maelicke, A. & Albuquerque, E. X. 2005. Memantine blocks α7* nicotinic acetylcholine receptors more potently than N-methyl-D-aspartate receptors in rat hippocampal neurons. *Journal of Pharmacology and Experimental Therapeutics,* 312**,** 1195-1205.

Atri, A., Molinuevo, J. L., Lemming, O., Wirth, Y., Pulte, I. & Wilkinson, D. 2013. Memantine in patients with Alzheimer's disease receiving donepezil: new analyses of efficacy and safety for combination therapy. *Alzheimer's research & therapy,* 5**,** 1-11.

Auld, D. S., Kornecook, T. J., Bastianetto, S. & Quirion, R. 2002. Alzheimer's disease and the basal forebrain cholinergic system: relations to β-amyloid peptides, cognition, and treatment strategies. *Progress in neurobiology,* 68**,** 209-245.

Bartus, R. T. 2000. On neurodegenerative diseases, models, and treatment strategies: lessons learned and lessons forgotten a generation following the cholinergic hypothesis. *Experimental neurology,* 163**,** 495-529.

Bekris, L. M., Yu, C.-E., Bird, T. D. & Tsuang, D. 2011. The Genetics of Alzheimer's Disease and Parkinson's Disease. *Neurochemical Mechanisms in Disease***,** 695-755.

Bezzerides, A. L., Mcgraw, K. J., Parker, R. S. & Husseini, J. 2007. Elytra color as a signal of chemical defense in the Asian ladybird beetle Harmonia axyridis. *Behavioral Ecology and Sociobiology,* 61**,** 1401-1408.

Birks, J. S. & Evans, J. G. 2015. Rivastigmine for Alzheimer's disease. *Cochrane Database of systematic reviews*.

Birks, J. S. & Harvey, R. J. 2018. Donepezil for dementia due to Alzheimer's disease. *Cochrane Database of systematic reviews*.

Blanke, M. L. & Vandongen, A. M. 2008. 13 Activation Mechanisms of the NMDA Receptor. *Biology of the NMDA Receptor***,** 283.

Bledsoe, D., Tamer, C., Mesic, I., Madry, C., Klein, B. G., Laube, B. & Costa, B. M. 2017. Positive modulatory interactions of NMDA receptor GluN1/2B ligand binding domains attenuate antagonists activity. *Frontiers in Pharmacology,* 8**,** 229.

Brackley, P., Bell, D., Choi, S., Nakanishi, K. & Usherwood, P. 1993. Selective antagonism of native and cloned kainate and NMDA receptors by polyamine-containing toxins. *Journal of Pharmacology and Experimental Therapeutics,* 266**,** 1573-1580.

Chen, H.-S. V. & Lipton, S. A. 2005. Pharmacological implications of two distinct mechanisms of interaction of memantine with N-methyl-D-aspartate-gated channels. *Journal of Pharmacology and Experimental Therapeutics,* 314**,** 961-971.

Chen, H. S. V. & Lipton, S. A. 2006. The chemical biology of clinically tolerated NMDA receptor antagonists. *Journal of neurochemistry,* 97**,** 1611-1626.

Danysz, W., Parsons, C. G., Möbius, H.-J., Stöffler, A. & Quack, G. 2000. Neuroprotective and symptomatological action of memantine relevant for Alzheimer's disease—a unified glutamatergic hypothesis on the mechanism of action. *Neurotoxicity research,* 2**,** 85-97.

Davies, P. & Maloney, A. 1976. Selective loss of central cholinergic neurons in Alzheimer's disease. *The Lancet,* 308**,** 1403.

De Ferrari, G. V., Canales, M. A., Shin, I., Weiner, L. M., Silman, I. & Inestrosa, N. C. 2001. A structural motif of acetylcholinesterase that promotes amyloid β-peptide fibril formation. *Biochemistry,* 40**,** 10447-10457.

Draper, B. 2013. *Understanding Alzheimer's disease and other dementias*, Jessica Kingsley Publishers.

Ellison, G. 1995. The N-methyl-D-aspartate antagonists phencyclidine, ketamine and dizocilpine as both behavioral and anatomical models of the dementias. *Brain Research Reviews,* 20**,** 250-267.

Erreger, K., Dravid, S. M., Banke, T. G., Wyllie, D. J. & Traynelis, S. F. 2005. Subunit-specific gating controls rat NR1/NR2A and NR1/NR2B NMDA channel kinetics and synaptic signalling profiles. *The Journal of physiology,* 563**,** 345-358.

Ezza, H. & Khadrawyb, Y. 2014. Glutamate excitotoxicity and neurodegeneration. *J Mol Genet Med,* 8**,** 1747-0862.1000141.

Farlow, M. R., Graham, S. M. & Alva, G. 2008. Memantine for the Treatment of Alzheimer's Disease. *Drug safety,* 31**,** 577-585.

Fendt, S.-M. & Verstreken, P. 2017. Neurons eat glutamate to stay alive. *The Journal of Cell Biology,* 216**,** 863.

Ferreira-Vieira, T., Guimaraes, I., Silva, F. & Ribeiro, F. 2016. Alzheimer's disease: targeting the cholinergic system. *Current neuropharmacology,* 14**,** 101-115.

Findley, C. A., Bartke, A., Hascup, K. N. & Hascup, E. R. 2019. Amyloid beta-related alterations to glutamate signaling dynamics during Alzheimer's disease progression. *ASN neuro,* 11**,** 1759091419855541.

Forette, F. & Hauw, J.-J. 2008. Alzheimer's disease: from brain lesions to new drugs. *Bulletin de L'academie Nationale de Medecine,* 192**,** 363-78; discussion 378.

Fotiou, D., Kaltsatou, A., Tsiptsios, D. & Nakou, M. 2015. Evaluation of the cholinergic hypothesis in Alzheimer's disease with neuropsychological methods. *Aging clinical and experimental research,* 27**,** 727-733.

Gielen, M., Retchless, B. S., Mony, L., Johnson, J. W. & Paoletti, P. 2009. Mechanism of differential control of NMDA receptor activity by NR2 subunits. *Nature,* 459**,** 703-707.

Gilling, K. E., Jatzke, C., Hechenberger, M. & Parsons, C. G. 2009. Potency, voltage-dependency, agonist concentration-dependency, blocking kinetics and partial untrapping of the uncompetitive N-methyl-D-aspartate (NMDA) channel blocker memantine at human NMDA (GluN1/GluN2A) receptors. *Neuropharmacology,* 56**,** 866-875.

Glasgow, N. G., Povysheva, N. V., Azofeifa, A. M. & Johnson, J. W. 2017. Memantine and ketamine differentially alter NMDA receptor desensitization. *Journal of Neuroscience,* 37**,** 9686-9704.

Grand, T., Abi Gerges, S., David, M., Diana, M. A. & Paoletti, P. 2018. Unmasking GluN1/GluN3A excitatory glycine NMDA receptors. *Nature communications,* 9**,** 1-12.

Hansen, K. B., Wollmuth, L. P., Bowie, D., Furukawa, H., Menniti, F. S., Sobolevsky, A. I., Swanson, G. T., Swanger, S. A., Greger, I. H. & Nakagawa, T. 2021. Structure, function, and pharmacology of glutamate receptor ion channels. *Pharmacological reviews,* 73**,** 298-487.

Hansen, K. B., Yi, F., Perszyk, R. E., Furukawa, H., Wollmuth, L. P., Gibb, A. J. & Traynelis, S. F. 2018. Structure, function, and allosteric modulation of NMDA receptors. *Journal of General Physiology,* 150**,** 1081-1105.

Hardingham, G. E. & Bading, H. 2003. The Yin and Yang of NMDA receptor signalling. *Trends in neurosciences,* 26**,** 81-89.

Hartmann, J. & Konnerth, A. 2005. Determinants of postsynaptic Ca2+ signaling in Purkinje neurons. *Cell calcium,* 37**,** 459-466.

Hedegaard, M., Hansen, K. B., Andersen, K. T., Bräuner-Osborne, H. & Traynelis, S. F. 2012. Molecular pharmacology of human NMDA receptors. *Neurochemistry international,* 61**,** 601-609.

Holtzman, D. M., Morris, J. C. & Goate, A. M. 2011. Alzheimer's disease: the challenge of the second century. *Science translational medicine,* 3**,** 77sr1-77sr1.

Huang, Y. H. & Bergles, D. E. 2004. Glutamate transporters bring competition to the synapse. *Current opinion in neurobiology,* 14**,** 346-352.

Huettner, J. E. 2015. Glutamate receptor pores. *The Journal of Physiology,* 593**,** 49-59.

Johnson, J. W., Glasgow, N. G. & Povysheva, N. V. 2015. Recent insights into the mode of action of memantine and ketamine. *Current opinion in pharmacology,* 20**,** 54-63.

Johnson, J. W. & Kotermanski, S. E. 2006. Mechanism of action of memantine. *Current opinion in pharmacology,* 6**,** 61-67.

Jones, K. S., Vandongen, H. M. & Vandongen, A. M. 2002. The NMDA receptor M3 segment is a conserved transduction element coupling ligand binding to channel opening. *Journal of Neuroscience,* 22**,** 2044-2053.

Julia, T. & Goate, A. M. 2017. Genetics of β-amyloid precursor protein in Alzheimer's disease. *Cold Spring Harbor perspectives in medicine,* 7**,** a024539.

Kaur, K. 2021. *The effect of memantine and the ladybird alkaloid, harmonine, on NMDA receptor function and Alzheimer's disease.* Neuroscience MRes MRes, University of Nottingham.

Kehoe, L. A., Bernardinelli, Y. & Muller, D. 2013. GluN3A: an NMDA receptor subunit with exquisite properties and functions. *Neural plasticity,* 2013.

Khan, U. A., Liu, L., Provenzano, F. A., Berman, D. E., Profaci, C. P., Sloan, R., Mayeux, R., Duff, K. E. & Small, S. A. 2014. Molecular drivers and cortical spread of lateral entorhinal cortex dysfunction in preclinical Alzheimer's disease. *Nature neuroscience,* 17**,** 304-311.

Kikuchi, T. 2020. Is Memantine Effective as an NMDA Receptor Antagonist in Adjunctive Therapy for Schizophrenia? *Biomolecules,* 10**,** 1134.

Kotermanski, S. E. & Johnson, J. W. 2009. Mg2+ imparts NMDA receptor subtype selectivity to the Alzheimer's drug memantine. *Journal of Neuroscience,* 29**,** 2774-2779.

Kotermanski, S. E., Wood, J. T. & Johnson, J. W. 2009. Memantine binding to a superficial site on NMDA receptors contributes to partial trapping. *The Journal of physiology,* 587**,** 4589-4604.

Kumar, A. 2015. NMDA receptor function during senescence: implication on cognitive performance. *Frontiers in neuroscience,* 9**,** 473.

Kumar, A., Gupta, V. & Sharma, S. 2021. Donepezil. *StatPearls [Internet].* StatPearls Publishing.

Kvist, T., Greenwood, J. R., Hansen, K. B., Traynelis, S. F. & Bräuner-Osborne, H. 2013. Structure-based discovery of antagonists for GluN3-containing N-methyl-D-aspartate receptors. *Neuropharmacology,* 75**,** 324-336.

Laferla, F. M., Martinez-Coria, H., Green, K. N. & Banerjee, P. K. 2009. P4-334: Combination of memantine and donepezil reverses cognitive deficits in transgenic mice with both amyloid-beta plaques and neurofibrillary tangles. *Alzheimer's & Dementia,* 5**,** e29-e29.

Limapichat, W., Yu, W. Y., Branigan, E., Lester, H. A. & Dougherty, D. A. 2013. Key binding interactions for memantine in the NMDA receptor. *ACS chemical neuroscience,* 4**,** 255-260.

Liu, J., Chang, L., Song, Y., Li, H. & Wu, Y. 2019. The role of NMDA receptors in Alzheimer's disease. *Frontiers in neuroscience***,** 43.

Magro, A., Ramon-Portugal, F., Facon, B., Ducamp, C. & Hemptinne, J. L. 2018. The evolution of chemical defenses along invasion routes: Harmonia axyridis Pallas (Coccinellidae: Coleoptera) as a case study. *Ecology and evolution,* 8**,** 8344-8353.

Maskell, P. D., Speder, P., Newberry, N. R. & Bermudez, I. 2003. Inhibition of human α7 nicotinic acetylcholine receptors by open channel blockers of N-methyl-D-aspartate receptors. *British journal of pharmacology,* 140**,** 1313-1319.

Mayer, M. L., Westbrook, G. L. & Guthrie, P. B. 1984. Voltage-dependent block by Mg2+ of NMDA responses in spinal cord neurones. *Nature,* 309**,** 261-263.

Mellor, I., Brier, T., Pluteanu, F., Strømgaard, K., Saghyan, A., Eldursi, N., Brierley, M., Andersen, K., Jaroszewski, J. & Krogsgaard-Larsen, P. 2003. Modification of the philanthotoxin-343 polyamine moiety results in different structure-activity profiles at muscle nicotinic ACh, NMDA and AMPA receptors. *Neuropharmacology,* 44**,** 70-80.

Monaghan, D. T. & Jane, D. E. 2009. Pharmacology of NMDA receptors. *Biology of the NMDA Receptor*.

Monyer, H., Burnashev, N., Laurie, D. J., Sakmann, B. & Seeburg, P. H. 1994. Developmental and regional expression in the rat brain and functional properties of four NMDA receptors. *Neuron,* 12**,** 529-540.

Mota, S. I., Ferreira, I. L. & Rego, A. C. 2014. Dysfunctional synapse in Alzheimer's disease–A focus on NMDA receptors. *Neuropharmacology,* 76**,** 16-26.

Mucke, L. & Selkoe, D. J. 2012. Neurotoxicity of amyloid β-protein: synaptic and network dysfunction. *Cold Spring Harbor perspectives in medicine,* 2**,** a006338.

Murpy, M. & Levine Iii, H. 2010. Alzheimer's disease and the β-amyloid peptide. *J Alzheimers Dis,* 19**,** 311-323.

Navarro, V., Sanchez-Mejias, E., Jimenez, S., Muñoz-Castro, C., Sanchez-Varo, R., Davila, J. C., Vizuete, M., Gutierrez, A. & Vitorica, J. 2018. Microglia in Alzheimer's disease: activated, dysfunctional or degenerative. *Frontiers in aging neuroscience***,** 140.

Niciu, M. J., Kelmendi, B. & Sanacora, G. 2012. Overview of glutamatergic neurotransmission in the nervous system. *Pharmacology Biochemistry and Behavior,* 100**,** 656-664.

Nicoll, R. & Malenka, R. 1999. Expression mechanisms underlying NMDA receptor-dependent long-term potentiation. *Annals of the new York Academy of Sciences,* 868**,** 515-525.

Nowak, L., Bregestovski, P., Ascher, P., Herbet, A. & Prochiantz, A. 1984. Magnesium gates glutamate-activated channels in mouse central neurones. *Nature,* 307**,** 462-465.

Nyakas, C., Granic, I., Halmy, L. G., Banerjee, P. & Luiten, P. G. 2011. The basal forebrain cholinergic system in aging and dementia. Rescuing cholinergic neurons from neurotoxic amyloid-β42 with memantine. *Behavioural Brain Research,* 221**,** 594-603.

Olivares, D., K Deshpande, V., Shi, Y., K Lahiri, D., H Greig, N., T Rogers, J. & Huang, X. 2012. N-methyl D-aspartate (NMDA) receptor antagonists and memantine treatment for Alzheimer's disease, vascular dementia and Parkinson's disease. *Current Alzheimer Research,* 9**,** 746-758.

Olney, J. W. 2003. Excitotoxicity, apoptosis and neuropsychiatric disorders. *Current opinion in pharmacology,* 3**,** 101-109.

Pająk, B., Kania, E. & Orzechowski, A. 2016. Killing me softly: connotations to unfolded protein response and oxidative stress in Alzheimer's disease. *Oxidative medicine and cellular longevity,* 2016.

Parsons, C. G., Danysz, W., Dekundy, A. & Pulte, I. 2013. Memantine and cholinesterase inhibitors: complementary mechanisms in the treatment of Alzheimer's disease. *Neurotoxicity research,* 24**,** 358-369.

Patel, R. 2017. *Investigating the pharmacology of ladybird alkaloids on ligand-gated ion channels.* University of Nottingham.

Patel, R. N., Richards, D. P., Duce, I. R., Birkett, M. A., Sattelle, D. B. & Mellor, I. R. 2020. Actions on mammalian and insect nicotinic acetylcholine receptors of harmonine-containing alkaloid extracts from the harlequin ladybird Harmonia axyridis. *Pesticide Biochemistry and Physiology,* 166**,** 104561.

Porsteinsson, A. P., Grossberg, G. T., Mintzer, J. & Olin, J. T. 2008. Memantine treatment in patients with mild to moderate Alzheimer's disease already receiving a cholinesterase inhibitor: a randomized, double-blind, placebo-controlled trial. *Current Alzheimer Research,* 5**,** 83-89.

Poulsen, M. H., Andersen, J., Christensen, R., Hansen, K. B., Traynelis, S. F., Strømgaard, K. & Kristensen, A. S. 2015. Binding of ArgTX-636 in the NMDA receptor ion channel. *Journal of molecular biology,* 427**,** 176-189.

Poulsen, M. H., Lucas, S., Bach, T. B., Barslund, A. F., Wenzler, C., Jensen, C. B., Kristensen, A. S. & Strømgaard, K. 2013. Structure–activity relationship studies of argiotoxins: selective and potent inhibitors of ionotropic glutamate receptors. *Journal of medicinal chemistry,* 56**,** 1171-1181.

Raschetti, R., Albanese, E., Vanacore, N. & Maggini, M. 2007. Cholinesterase inhibitors in mild cognitive impairment: a systematic review of randomised trials. *PLoS medicine,* 4**,** e338.

Richards, D. 2011. *Investigating ladybird (Coleoptera: Coccinellidae) alkaloids as novel sources for insecticides: differential inhibition of the vertebrate and invertebrate nicotinic acetylcholine receptor using harlequin ladybird (Harmonia axyridis) extract and synthetic hippodamine.* University of Nottingham.

Röhrich, C. R., Ngwa, C. J., Wiesner, J., Schmidtberg, H., Degenkolb, T., Kollewe, C., Fischer, R., Pradel, G. & Vilcinskas, A. 2012. Harmonine, a defence compound from the harlequin ladybird, inhibits mycobacterial growth and demonstrates multi-stage antimalarial activity. *Biology letters,* 8**,** 308-311.

Rosini, M., Simoni, E., Bartolini, M., Cavalli, A., Ceccarini, L., Pascu, N., Mcclymont, D. W., Tarozzi, A., Bolognesi, M. L. & Minarini, A. 2008. Inhibition of acetylcholinesterase, β-amyloid aggregation, and NMDA receptors in Alzheimer's disease: a promising direction for the multi-target-directed ligands gold rush. *Journal of medicinal chemistry,* 51**,** 4381-4384.

Rosini, M., Simoni, E., Bartolini, M., Soriano, E., Marco-Contelles, J., Andrisano, V., Monti, B., Windisch, M., Hutter-Paier, B. & Mcclymont, D. W. 2013. The bivalent ligand approach as a tool for improving the in vitro anti-Alzheimer multitarget profile of dimebon. *ChemMedChem,* 8**,** 1276-1281.

Rothstein, J. D., Martin, L., Levey, A. I., Dykes-Hoberg, M., Jin, L., Wu, D., Nash, N. & Kuncl, R. W. 1994. Localization of neuronal and glial glutamate transporters. *Neuron,* 13**,** 713-725.

Roy, H. & Wajnberg, E. 2008. From biological control to invasion: the ladybird Harmonia axyridis as a model species. *BioControl,* 53**,** 1-4.

Sasaki, Y. F., Rothe, T., Premkumar, L. S., Das, S., Cui, J., Talantova, M. V., Wong, H.-K., Gong, X., Chan, S. F. & Zhang, D. 2002. Characterization and comparison of the NR3A subunit of the NMDA receptor in recombinant systems and primary cortical neurons. *Journal of neurophysiology,* 87**,** 2052-2063.

Seago, A. E., Giorgi, J. A., Li, J. & Ślipiński, A. 2011. Phylogeny, classification and evolution of ladybird beetles (Coleoptera: Coccinellidae) based on simultaneous analysis of molecular and morphological data. *Molecular Phylogenetics and Evolution,* 60**,** 137-151.

Selkoe, D. J. 2002. Alzheimer's disease is a synaptic failure. *Science,* 298**,** 789-791.

Selkoe, D. J. & Hardy, J. 2016. The amyloid hypothesis of Alzheimer's disease at 25 years. *EMBO molecular medicine,* 8**,** 595-608.

Sims, N., Bowen, D., Allen, S., Smith, C., Neary, D., Thomas, D. & Davison, A. 1983. Presynaptic cholinergic dysfunction in patients with dementia. *Journal of neurochemistry,* 40**,** 503-509.

Sloggett, J. & Davis, A. 2010. Eating chemically defended prey: alkaloid metabolism in an invasive ladybird predator of other ladybirds (Coleoptera: Coccinellidae). *Journal of Experimental Biology,* 213**,** 237-241.

Sobolevsky, A. I., Rosconi, M. P. & Gouaux, E. 2009. X-ray structure of AMPA-subtype glutamate receptor: symmetry and mechanism. *Nature,* 462**,** 745.

Song, X., Jensen, M. Ø., Jogini, V., Stein, R. A., Lee, C.-H., Mchaourab, H. S., Shaw, D. E. & Gouaux, E. 2018. Mechanism of NMDA receptor channel block by MK-801 and memantine. *Nature,* 556**,** 515-519.

Stephenson, F. 2006. Structure and trafficking of NMDA and GABAA receptors. Portland Press Ltd.

Stern-Bach, Y., Bettler, B., Hartley, M., Sheppard, P. O., O'hara, P. J. & Heinemann, S. F. 1994. Agonist selectivity of glutamate receptors is specified by two domains structurally related to bacterial amino acid-binding proteins. *Neuron,* 13**,** 1345-1357.

Tariot, P. N., Farlow, M. R., Grossberg, G. T., Graham, S. M., Mcdonald, S., Gergel, I., Group, M. S. & Group, M. S. 2004. Memantine treatment in patients with moderate to severe Alzheimer disease already receiving donepezil: a randomized controlled trial. *Jama,* 291**,** 317-324.

Terry, A. V. & Buccafusco, J. J. 2003. The cholinergic hypothesis of age and Alzheimer's disease-related cognitive deficits: recent challenges and their implications for novel drug development. *Journal of Pharmacology and Experimental Therapeutics,* 306**,** 821-827.

Traynelis, S. F., Wollmuth, L. P., Mcbain, C. J., Menniti, F. S., Vance, K. M., Ogden, K. K., Hansen, K. B., Yuan, H., Myers, S. J. & Dingledine, R. 2010. Glutamate receptor ion channels: structure, regulation, and function. *Pharmacological reviews,* 62**,** 405-496.

Vieira, M., Yong, X. L. H., Roche, K. W. & Anggono, V. 2020. Regulation of NMDA glutamate receptor functions by the GluN2 subunits. *Journal of neurochemistry,* 154**,** 121-143.

Vilcinskas, A., Stoecker, K., Schmidtberg, H., Röhrich, C. R. & Vogel, H. 2013. Invasive harlequin ladybird carries biological weapons against native competitors. *Science,* 340**,** 862-863.

Villemagne, V. L., Doré, V., Burnham, S. C., Masters, C. L. & Rowe, C. C. 2018. Imaging tau and amyloid-β proteinopathies in Alzheimer disease and other conditions. *Nature Reviews Neurology,* 14**,** 225-236.

Vogel, J. W., Iturria-Medina, Y., Strandberg, O. T., Smith, R., Levitis, E., Evans, A. C. & Hansson, O. 2020. Spread of pathological tau proteins through communicating neurons in human Alzheimer's disease. *Nature communications,* 11**,** 1-15.

Watanabe, J., Beck, C., Kuner, T., Premkumar, L. S. & Wollmuth, L. P. 2002. DRPEER: a motif in the extracellular vestibule conferring high Ca2+ flux rates in NMDA receptor channels. *Journal of Neuroscience,* 22**,** 10209-10216.

Waxman, E. A. & Lynch, D. R. 2005. N-methyl-D-aspartate receptor subtypes: multiple roles in excitotoxicity and neurological disease. *The Neuroscientist,* 11**,** 37-49.

Wilkinson, D., Murray, J. I. & Group, G. R. 2001. Galantamine: a randomized, double-blind, dose comparison in patients with Alzheimer's disease. *International journal of geriatric psychiatry,* 16**,** 852-857.

Witt, A., Macdonald, N. & Kirkpatrick, P. 2004. Memantine hydrochloride. *Nat Rev Drug Discov,* 3**,** 109-110.

Wollmuth, L. P. 2019. Prying open a glutamate receptor gate. *Journal of General Physiology,* 151**,** 396-399.

Wollmuth, L. P. & Sobolevsky, A. I. 2004. Structure and gating of the glutamate receptor ion channel. *Trends in neurosciences,* 27**,** 321-328.

Wolosker, H. 2006. D-serine regulation of NMDA receptor activity. *Science's STKE,* 2006**,** pe41-pe41.

Woodhull, A. M. 1973. Ionic blockage of sodium channels in nerve. *The Journal of general physiology,* 61**,** 687-708.

Wyllie, D., Livesey, M. & Hardingham, G. 2013. Influence of GluN2 subunit identity on NMDA receptor function. *Neuropharmacology,* 74**,** 4-17.

Yamakura, T. & Shimoji, K. 1999. Subunit-and site-specific pharmacology of the NMDA receptor channel. *Progress in neurobiology,* 59**,** 279-298.

Yin, Y. I., Bassit, B., Zhu, L., Yang, X., Wang, C. & Li, Y.-M. 2007. γ-Secretase substrate concentration modulates the Aβ42/Aβ40 ratio: Implications for Alzheimer disease. *Journal of Biological Chemistry,* 282**,** 23639-23644.

Yuan, H., Hansen, K. B., Vance, K. M., Ogden, K. K. & Traynelis, S. F. 2009. Control of NMDA receptor function by the NR2 subunit amino-terminal domain. *Journal of Neuroscience,* 29**,** 12045-12058.

Zhang, Y., Li, P., Feng, J. & Wu, M. 2016. Dysfunction of NMDA receptors in Alzheimer's disease. *Neurological Sciences,* 37**,** 1039-1047.

Zuo, J., De Jager, P. L., Takahashi, K. A., Jiang, W., Linden, D. J. & Heintz, N. 1997. Neurodegeneration in Lurcher mice caused by mutation in δ2 glutamate receptor gene. *Nature,* 388**,** 769-773.